DIAGNOSIS OF SELECTED HUMAN EYE DISEASES USING ARTIFICIAL NEURAL NETWORKS

BY

FANIJO, SAMUEL OLAWALE

CPE/12/0885

An Undergraduate Project Submitted to

the department of Computer Engineering,

Faculty of Engineering,

Federal University Oye- Ekiti (FUOYE), Ekiti, Nigeria,

IN PARTIAL FULFILLMENT OF THE REQUIREMENTS FOR THE AWARD OF THE DEGREE OF BACHELOR OF ENGINEERING (B.ENG) IN COMPUTER ENGINEERING.

December, 2017

CERTIFICATION

This project with the title

DIAGNOSIS OF SELECTED HUMAN EYE DISEASES USING ARTIFICIAL NEURAL NETWORKS

Submitted by

FANIJO, SAMUEL OLAWALE (CPE/12/0885)

Has satisfied the regulations governing the award of degree of

BACHELOR OF ENGINEERING (B.Eng) IN COMPUTER ENGINEERING,

Federal University Oye-Ekiti, Nigeria.

.....
Dr. (Engr) I.A. Adeyanju
Supervisor

20-12-2017
.....
Date

DEPARTMENT OF COMPUTER ENGINEERING
HOD SIGN
DATE 20/12/17
FEDERAL UNIVERSITY OYE EKITI

.....
Dr. (Engr) I.A. Adeyanju
Head of Department

20-12-2017
.....
Date

DECLARATION

This project is a result of my own work and has not been copied in part or in whole from any other source except where duly acknowledged. As such, all use of previously published work (from books, journals, internet etc.) has been acknowledged within the main report to an entry in the References list.

COPYRIGHT

Fani-Jo Samuel O.
.....
Student's Full Name

.....
Signature & Date

DEDICATION

I dedicate this project to my father, the Almighty God – The Alpha and Omega of my life and my amiable mother, Mrs. Comfort Foluke Fanijo.

ACKNOWLEDGEMENTS

I remain thankful to the Almighty God who lifts up my head and sustains His grace and glory upon my life. My immense acknowledgement goes to my ever supportive Supervisor and Head of Department, Dr. (Engr.) I.A. Adeyanju, my level adviser, Engr. N.S. Okomba, the departmental Project coordinator, Dr. (Engr.) O.M. Olaniyan, and also not forgetting Dr. (Engr.) A.S. Falohun for his most respected comments and guidance as well as the entire staff of the department of Computer Engineering, Federal University Oye-Ekiti.

Furthermore, I am indeed very grateful to my loving mother, Mrs C.F. Fanijo for her parental support, prayers, encouragement and guidance since my birth. I also acknowledge and appreciate my most respected brother - Cornelius Adewale, because he has always been there; and not also forgetting Joseph and Ebenezer Fanijo, my sweet siblings. Finally, special thanks goes to Adewale Ayodele, Raheem Waliu, Jayeoba Monisola, and my other departmental mates who have been very helpful and supportive, I acknowledge all your support.

ABSTRACT

The human eye is a vital organ of vision, which gives us the sense of sight, and is of utmost importance in all day to day activities. However, there are many diseases that affect the human eye and can lead to blindness. The major causes of blindness include glaucoma, diabetic retinopathy and other corneal and retinal infections. However, most of these conditions can be prevented with an early diagnosis. There are several techniques of diagnosis in digital health which can be used for early detection of blindness by analyzing fundus images. These includes K-Nearest Neighbor algorithm (KNN), Support Vector Machine (SVM) and Artificial Neural Networks (ANN). Artificial Neural Networks has the advantage of accuracy in problem-solving, adaptive nature of learning, fault tolerance and real time operational mode quality over others. This project presents an Artificial Neural Network (ANN) based system to detect Glaucoma and Diabetic Retinopathy by automatically analyzing fundus eye images of suspected patients.

The implementation of this project was done in four (4) modules. Data acquisition was done via publicly available online fundus database, and the database used includes Hossein Rabbani, SPIE, and ORIGA-light fundus database. The acquired fundus images were passed through Preprocessing stage. The preprocessing techniques used were grayscale, histogram equalization, and thresholding. Feature extraction was done using Gray Levels Co-occurrence Matrix (GLCM) and four textural features were extracted from each fundus image in form of positive integers. The four features are: Contrast, Correlation, Energy and Homogeneity. These four features served as the input into a Back Propagation Neural Network. The Back Propagation Neural Network (BPNN) is mostly popular for its ability to minimize errors in classification. The Hidden Layer configuration used in the BPNN for the training were two hidden layers and three hidden neurons each (fed into each layer) at a threshold value '0.6'.

The developed system was trained on a total of 135 fundus images, while 60 fundus images were used for proper testing and evaluation of the developed system. An accuracy of 90% was obtained for Diabetic Retinopathy; 95% obtained for Glaucoma; and 100% obtained for the Healthy class. The overall accuracy for the developed system was found to be 95%, coupled with the fact that it only takes about 13 seconds to screen one eye; as opposed to manual screening which takes about 15 to 20 minutes.

The developed ANN-based eye diseases decision support system will assist in screening diabetic retinopathy and glaucoma. This will greatly assist ophthalmologists with early diagnosis; Hence, the system has the potential to reduce the possibility of vision loss or blindness.

2.3.4 Age-related Macula Degeneration.....22
2.3.5 Retinoblastoma.....23
2.4 Eye Image Acquisition.....24
2.4.1 Fundus Imaging.....24
2.4.2 Hyperspectral Imaging.....25
2.4.3 Scanning Laser Ophthalmoscopy.....26
2.5 Image Pre-processing Techniques.....27
2.5.1 Gray Scale Conversion.....27
2.5.2 Thresholding.....29
2.5.3 Adaptive Histogram Equalization.....30
2.5.4 Gaussian Filter.....31
2.5.5 Morphological Operations.....33
2.6 Feature Extraction Techniques.....34
2.6.1 Gray-level Co-occurrence Matrix.....35
2.6.2 Gabor Filter.....37
2.6.3 Principal Component Analysis.....38
2.7 Machine Learning Algorithms for Digital Health.....39
2.7.1 K-Nearest Neighbor Algorithm.....39
2.7.2 Artificial Neural Networks.....40
2.7.3 Fuzzy Logic.....42
2.7.4 Support Vector Machine.....43
2.7.5 Hidden Markov Model.....44
2.8 Related Works.....45
CHAPTER THREE - METHODOLOGY 50
3.1 Overview of the Eye Diseases Diagnostic System.....50
3.2 Data Acquisition.....51
3.2.1 Hossein Rabbani Eye Fundus Database.....51
3.2.2 SPIE Eye Fundus Database.....52

3.2.3 Jan Odstrcilik Eye Fundus Database.....52

3.2.4 ORIGA-light Eye Fundus Database.....53

3.3 Image Pre-processing 54

3.3.1 Conversion to Grayscale.....54

3.3.2 Histogram Equalization.....55

3.3.3 Thresholding.....56

3.4 Feature Extraction using GLCM.....57

3.4.1 Contrast.....57

3.4.2 Correlation.....57

3.4.3 Energy.....57

3.4.4 Homogeneity.....58

3.5 Diagnosis/Classification Artificial Neural Networks.....58

3.5.1 Training and Detection of Eye Disease using Back Propagation Neural Network (BPNN).....58

3.5.2 Hidden Layer and Neuron.....59

3.5.3 Threshold Function.....59

3.6 Experimental Setup.....63

3.7 Performance Evaluation of the Eye Disease Diagnostic System.....64

CHAPTER FOUR - IMPLEMENTATION AND RESULTS 65

4.1 Implementation.....65

4.2 Determination of Neural Network parameters.....65

4.2.1 Determination of Hidden Layer Configuration.....66

4.2.2 Determination of Threshold Value.....69

4.3 Classification Results with Optimal Neural Network Parameters.....73

4.4 Further Discussion.....74

4.5 Performance Comparison with Similar System.....76

CHAPTER FIVE - CONCLUSION AND RECOMMENDATIONS 78

5.1 Summary.....78

5.2 Conclusion.....79

5.3 Recommendations.....79

LIST OF FIGURES

FIGURE	PAGE
2.1: Anatomy of the eye	14
2.2: Cataract fundus image	19
2.3: Glaucoma fundus image	20
2.4: DR fundus image	21
2.5: AMD fundus image	23
2.6: Retinoblastoma fundus image	24
2.7: Fundus image of a normal eye	25
2.8: Hyperspectral imaging	26
2.9: Scanning laser ophthalmology	27
2.10: Gray-scale converted image	29
2.11: Fundus image after thresholding	30
2.12: Contrast enhancement by adaptive histogram equalization	31
2.13: Smoothing by Gaussian filter	32
2.14: Dilation and erosion	34
2.15: Multilayered feed forward artificial neural networks	41
3.1: Overview of Proposed Ann-Based Human Eye Diseases Diagnostic System	50
3.2: Diabetic fundus images acquired from Hossein Rabbani eye fundus database	51
3.3: Healthy fundus images sample acquired from the SPIE database	52
3.4: Diabetic and Glaucomatous fundus images acquired from the Jan Odstrcilik database	53
3.5: Glaucomatous fundus images sample acquired from the ORIGA-Light database	53

3.5: Glaucomatous fundus images sample acquired from the ORIGA-Light database 53

3.6: Fundus image before and after gray scale preprocessing 55

3.8: Graphical description of all preprocessing techniques used. 56

3.9: Description of the Neural network during training phase 61

3.10: Flowchart showing training and testing phase for the diagnostic system with BPNN 62

4.1: GUI display for software implementation. 64

4.2: Confusion matrices of NN for different hidden layer configurations at threshold 0.9 68

4.3: Confusion matrices of NN for nine threshold values 72

4.4: Confusion matrices for classification test results 74

LIST OF TABLES

TABLE	PAGE
4.1: System performance results for different NN parameters	66
4.2: System performance for different NN parameters	69
4.3: System classification test results accuracy	73
4.4: Performance Evaluation Results	75
4.5: Performance comparison between the developed system and similar existing systems	77

LIST OF ACRONYMS

AIM:	Artificial Intelligence in Medicine
AHE:	Adaptive Histogram Equalization
ANN:	Artificial Neural Networks
AI:	Artificial Intelligence
AMD:	Age-related Macula Degeneration
BPNN:	Back Propagation Neural Network
CBT:	Computer Based Test
CLAHE:	Contrast Limited Adaptive Histogram Equalization
CDR:	Cup-to-Disk Ratio
DR:	Diabetic Retinopathy
EHR:	Electronic Health Record
FNR:	False Negative Rate
FPR:	False Positive Rate
FP:	False Positive
FN:	False Negative
GLCM:	Gray-Level Co-occurrence Matrix
GUI:	Graphical User Interface
HL:	Hidden Layer
HRT:	Heidelberg Retina Tomography
HMM:	Hidden Markov Model

ICT:	Information and Communication Technology
IOP:	Intra-ocular pressure
KNN:	K-Nearest Neighborhood Algorithm
MRF:	Markov Random Field
NN:	Neural Network
ONH:	Optic Nerve Head
PCA:	Principal Component Analysis
RGB:	Red, Green, Blue
SLO:	Scanner Laser Ophthalmoscopy
SVM:	Support Vector Machine
TP:	True Positive
TN:	True Negative
WHO:	World-Health-Organization

CHAPTER ONE

INTRODUCTION

1.1 Preamble

Digital health is an emerging field in the intersection of medical informatics, public health and business, referring to health services and information delivered or enhanced through the Internet and related technologies (Eysenbach, 2001). In a broader sense, the term characterizes not only a technical development, but also a state-of-mind, a way of thinking, an attitude, and a commitment for networked, global thinking, to improve healthcare locally, regionally, and worldwide by using information and communication technology (Eysenbach, 2001). Digital health encompasses a wide variety of domain, which includes Artificial Intelligence in Medicine (AIM.), Electronic Health Records (EHR.), Clinical Point of Care, Mobile Health (mHealth), as well as Telemedicine. (Wright & Wright, 1997).

Artificial intelligence in Medical field emerged in the early 1970's in response to several simultaneous needs, opportunities and interests (Javitt, 1986). An increased demand for high quality medical services coupled with the explosive growth of medical knowledge has led to the usage of computer program that could be used to assist physicians and other health care providers in discharging their clinical roles in diagnosis, therapy and prognosis (Javitt, 1986). Artificial intelligence (AI) field began to reach its maturity when first applied for representation and reasoning in medical diagnosis in areas such as thyroid diseases, breast diseases, drug poisoning, electrolyte disorder, jaundice and liver dysfunctions, ventilator management, pulmonary function, hematology, chest pain, ophthalmology and oncology (Szolovits, 1982). Digital health systems reduce clinical errors and improve evidence-based medicine by increasing the accuracy of diagnoses, earliness of the diagnosis as well as the appropriateness of treatment approaches.

The human eye is a vital organ of vision, which gives us the sense of sight, and is of utmost importance in all day to day activities. However, there are many diseases that affect the human eye and can lead to

blindness. The major causes of blindness include glaucoma, diabetic retinopathy and other corneal and retinal infections (Oliveira, 2014). It is estimated that in the world there are approximately 1.5 million blind children (WHO, 2015), while there are about 285million people, in total, estimated to be blind worldwide; of which 82% of them are aged 50 above (WHO, 2015). One of the five priorities of the World Health Organization is to tackle blindness, especially in children (WHO, 2015), and the role of digital health in actualizing this priority cannot be overemphasized. This project proposes a digital health system to diagnose selected human eye diseases using Artificial Neural Network.

1.2 Statement of the Problem

According to a survey carried out by the World Health Organization (2015), it is estimated that in the world there are approximately 1.5 million blind children, with a further 1.2 million representing the number of blind people between the age range of 40 and 50; while a further 2.7million adults aged 50 years and above are estimated to have moderate visual impairment. Furthermore, one of the most common diseases that has affected people aged above 50 years is age related macular degeneration, which is currently responsible for about 4.25million blind Nigerians (WHO, 2015). Thus, patients in their fifties or more who have undergone surgery for glaucoma are mostly advised to always have their eyes examined annually.

Inspection provides a large number of fundus images and medical professionals have to continually peruse them spending valuable time and energy, however, current methods of detection and assessment of eye disease are manual, expensive and potentially inconsistent. Therefore, it would be more cost effective and beneficial if the initial task of analyzing retinal (fundus) images are automated (Manoujitha & Goonetileke, 2014). Such a system would act as an early detection and warning system, where a person can actually get diagnosed in order to prevent extreme conditions or blindness. It can also assist an ophthalmologist to analyze numerous images within a brief period and spend more time on those patients whose cases require further investigation (Manoujitha & Goonetileke, 2014).

There are several techniques of diagnosis in digital health which can be used for early detection of blindness by analyzing fundus images. These includes K-Nearest Neighbor algorithm (KNN), Support Vector Machine (SVM) and Artificial Neural Networks (ANN) (Karegowda *et al.,* 2011). KNN is robust especially while dealing with noisy data and also effective if the training data is large, however its major bottleneck is the task of determining the value of the parameter "K" (Alamelu *et al.,* 2015). The merits of SVM includes the regularization parameter, which makes the user think about avoiding over-fitting as well as the kernel trick, which helps build in expert knowledge about a problem via engineering of the kernel. However, the major drawback in SVM is that the theory only really covers the determination of the parameters for a given value of the regularization, kernel parameters and choice of kernel (Alamelu, 2015).

Artificial Neural Networks has the advantage of accuracy in problem-solving, adaptive nature of learning, fault tolerance and real time operational mode quality over others (Karegowda *et al.,* 2011); all of which contributes to its' selection as the tool used in this project for the diagnosis of selected human eye diseases by automatically analyzing fundus eye images of suspected patients.

1.3 Aim and Objectives

The aim of this project is to develop a Human Eye-disease Diagnostic System using Artificial Neural Network. The specific objectives are:

1. To design a diagnostic system for the detection of selected eye diseases based on Artificial Neural Network.

2. To implement the diagnostic system using MATLAB Software.

3. To evaluate the effectiveness and efficiency of the developed system.

1.4 Methods of Study

The methods to be used in achieving this project will include the following:

i. Continual review of relevant literatures and online resources related to Artificial Neural networks, Diagnosis of eye diseases using ANN, Digital Health, Feature Extraction, and Image Processing.

ii. Interaction with Ophthalmologists and experts in Neural Networks.

iii. Techniques of implementing ANN architecture into a system will be studied and further implemented appropriately at the design stage.

iv. Design of the ANN-based human eye diseases diagnostic system.

v. Data Acquisition from publicly available online databases (in form of fundus images) will be carried out in order to train and test the network appropriately.

vi. The data acquired will be preprocessed appropriately.

vii. Feature extraction will be done on the preprocessed fundus images.

viii. Implementation of the system using an Artificial Neural Network classifier, trained using extracted features from fundus images.

ix. Evaluation of the implemented ANN-based Human-Eye Diagnostic System will be carried out.

1.5 Scope of the Study

This project will develop a Human Eye Diagnostic System based on Artificial Neural Networks for two eye diseases. However, only diseases diagnosable from eye fundus images will be considered in this project. The proposed diagnostic system will make use of ANN. Other classifiers such as fuzzy logic, Support Vector Machine (SVM) and K-Nearest Neighborhood Algorithm (KNN) can also be used but are not considered in this project.

1.6 Significance of Study

In the promotion of how health services are delivered to the public in need, the role of digital health cannot be overemphasized. Areas which digital health is applied includes:

- **Clinical Decision Support Systems (CDSS):** A clinical decision-support system is any computer program designed to help healthcare professionals to make clinical decisions. In a sense, any computer system that deals with clinical data or knowledge, (such as the proposed system in this project) is intended to provide decision support. Clinical Decision Support Systems are one of the most prominent examples of the role Medical Informatics may have in the improvement of health care (Musen, 2000). The ability to provide advice at different moments and in various situations of the clinical process, may it be to a physician, a nurse, or an assistant caregiver, tailored to the condition of a specific patient, has the potential to significantly improve the quality of care delivery.
- **Electronic Health Records (EHR):** Patient data stored on computers enabling the communication of patient data between different health care professionals. The essence of Electronic health records includes (Mantas, 2002): to improve the accuracy and quality of data recorded in a health record; enhance health practitioners' access to a patient's healthcare information enabling it to be shared by all for the present and continuing care of that patient; improve the quality of care as a result of having health information immediately available at all times for patient care; and as well improve the efficiency of the health record service.
- **Telemedicine:** Telemedicine involves the physical and psychological treatments provided over networks, including telemonitoring of patients' functions. Telemedicine is the use of medical information exchanged from one site to another via electronic communications to improve patients' health status (Strehle & Shabde, 2006). Closely associated with telemedicine is the term "telehealth," which is often used to encompass a broader definition of remote healthcare

that does not always involve clinical services. Videoconferencing, transmission of still images, e-health including patient portals, remote monitoring of vital signs, continuing medical education and nursing call centers are all considered part of telemedicine and telehealth (Rao & Lombardi, 2005).

- **M-health:** M-health includes the use of mobile devices in collecting aggregate and patient-level health data; providing health care information to practitioners, researchers and patients; real-time monitoring of patient vitals; and direct provision of care via mobile telemedicine (Iluyemi *et al.,* 2012). Mobile devices and tablets provide accessibility to the Electronic Medical Record during the clinical point of care documentation process. Mobile technologies such as Android phones, iPhones, BlackBerrys, and tablets feature touchscreens to further support the ease of use for the physicians. Furthermore, mobile electronic records application supports workflow portability needs, through which clinicians can document patient information at the patient's bedside at any point in time (Iluyemi *et al.,* 2012).
- **Health knowledge management:** This involves the provision of overview of latest medical journals, best practice guidelines or epidemiological tracking (for example, physician resources such as Medscape). Health knowledge management also includes the use of software solutions for appointment scheduling, patient data management, work schedule management and other administrative tasks surrounding health (Iluyemi *et al.,* 2012).

CHAPTER TWO

LITERATURE REVIEW

2.1 Digital Health

The explosion of information and communication technology (ICT) advances over the past two decades has made a significant impact on all aspects of our lives – the way we think, the way we socialize, the way we listen to music – the way we exist. The world is at a point in time where four major digital developments – mobile phones, personal computers, the internet and social networking – are now interlocked to revolutionize our lives (Kariyawasam *et al.*, 2010). According to The Kariyawasam et al. (2010), mobile phones have made a bigger difference to the lives of more people, more quickly than any other technology. In like manner, the world of health is also being impacted, but the full depth and scope of the potential of ICTs has not yet been fully explored in the field of medicine. With increasing worldwide connectivity and mobile penetration reaching even into developing countries, digital health has become a powerful tool in the hands of medical professionals and the public (Kariyawasam *et al.*, 2010).

"Digital health is an emerging field in the intersection of medical informatics, public health and business, referring to health services and information delivered or enhanced through the internet and related technologies" (Iluyemi *et al.*, 2012). In a broader sense, the term characterizes not only a technical development, but also a state of mind, a way of thinking, an attitude and a commitment for networked, global thinking, to improve health care locally, regionally and worldwide by using information and communication technology. Digital health has found various applications in the field of medicine and such applications includes electronic health records, telemedicine, digital therapy, as well as artificial intelligence in medicine (Iluyemi *et al.*, 2012).

2.1.1 Electronic Health Record (EHR)

With the many advances in information technology over the past 20 years, particularly in healthcare, a number of different forms of electronic health records (EHR) have been discussed, developed, and implemented (WHO, 2006a). Some institutions/countries are currently planning the introduction of a nationwide electronic health record while others have actually implemented some form of EHR. However, the type and extent of electronic health records vary and what one country calls an EHR may not be the same as that developed in another country. Although work has been undertaken by institutions/countries on some form of a computerized patient healthcare information system, as yet not many hospitals have successfully introduced an electronic health record with clinical data entry at the point of care. However, institutions should not focus on just going paperless, but rather should focus also on encouraging departments and healthcare practitioners to move to an electronic system to help improve the accuracy of data recorded in a health record, enhance the health practitioners' access to a patient's healthcare information; improve the quality of patient's care and boost the overall efficiency of the health record service (WHO, 2006a).

Although interest in automating the health record is generally high in both developed and developing countries, unfortunately, in some cases, the introduction of an EHR system seems overwhelming. In addition, the EHR is almost out of reach to many healthcare providers and administrators as well as medical record/health information managers (WHO, 2006b). The obstacles may not be available technology but a problem of technical support and the cost of changing to an electronic system coupled with insufficient healthcare funding. In many developing countries, costs, available technology, lack of technical expertise and computer skills of staff, and lack of data processing facilities are major issues which would need to be addressed before implementation is possible (WHO, 2006b).

2.1.2 Telemedicine

Telemedicine, a term coined in the 1970s, which literally means "healing at a distance" (Sood, 2006), signifies the use of ICT to improve patient outcomes by increasing access to care and medical information. Recognizing that there is no one definitive definition of the word 'telemedicine', a 2007 study found 104 peer-reviewed definitions of the word, which subsequently lead to a conventional adoption of a broad description of it as being "The delivery of health care services, where distance is a critical factor, by all health care professionals using information and communication technologies for the exchange of valid information for diagnosis, treatment and prevention of disease and injuries, research and evaluation, and for the continuing education of health care providers, all in the interests of advancing the health of individuals and their communities" (WHO, 2007).

In a nutshell, Telemedicine is the use of medical information exchanged from one site to another via electronic communications to improve patients' health status. Closely associated with telemedicine is the term "telehealth," which is often used to encompass a broader definition of remote healthcare that does not always involve clinical services. Videoconferencing, transmission of still images, e-health including patient portals, remote monitoring of vital signs, continuing medical education and nursing call centers are all considered part of telemedicine and telehealth (Rao *et al.,* 2005).

The many definitions highlight that telemedicine is an open and constantly evolving science, as it incorporates new advancements in technology and responds and adapts to the changing health needs and contexts of societies. Some distinguish telemedicine from telehealth with the former restricted to service delivery by physicians only, and the latter signifying services provided by health professionals in general, including nurses, pharmacists, and others. However, at the end of the day, it can always be said that telemedicine and telehealth are synonymous and used interchangeably. There are four elements that are germane to telemedicine (WHO, 2007). These elements includes: the provision of

clinical support; overcoming of geographical barriers, the use of various types of ICT; and improvement of health outcomes.

Telemedicine applications can be classified into two basic types, according to the timing of the information transmitted and the interaction between the individuals involved: health professional-to-health professional or health professional-to-patient (Einthoven, 2005). Store-and-forward, or asynchronous, telemedicine involves the exchange of pre-recorded data between two or more individuals at different times. For example, the patient or referring health professional sends an e-mail description of a medical case to an expert who later sends back an opinion regarding diagnosis and optimal management (Wootton *et al.,* 2009). In contrast, real time, or synchronous, telemedicine requires the involved individuals to be simultaneously present for immediate exchange of information, as in the case of videoconferencing (Wootton *et al.,* 2009). In both synchronous and asynchronous telemedicine, relevant information may be transmitted in a variety of media, such as text, audio, video, or still images. These two basic approaches to telemedicine are applied to a wide array of services in diverse settings, including teledermatology, telepathology, and teleradiology (Wootton, 2009).

The majority of telemedicine services, most of which focus on diagnosis and clinical management, are routinely offered in industrialized regions including, but not limited to the United Kingdom of Great Britain and Northern Ireland, Scandinavia, North America, and Australia (Heinzelmann *et al.,* 2000; Einthoven, 2005). In addition, biometric measuring devices such as equipment monitoring heart rate, blood pressure and blood glucose levels are increasingly used to remotely monitor and manage patients with acute and chronic illnesses. Some predict that telemedicine will profoundly transform the delivery of health services in the industrialized world by migrating health care delivery away from hospitals and clinics into homes (Wootton, 2005).

In low-income countries and in regions with limited infrastructure, telemedicine applications are primarily used to link health-care providers with specialists, referral hospitals, and tertiary care centres (Wootton, 2005). Even though low-cost telemedicine applications have proven to be feasible, clinically useful, sustainable, and scalable in such settings and underserved communities, these applications are not being adopted on a significant scale due to a variety of barriers such as physician licensing and credentialing (Wootton, 2009).

2.1.3 Digital Therapy

Digital therapy is an emerging and fast developing field of research and practice that involves the application of digital technologies to assist or deliver psychotherapy (Wright *et al.,* 1997). Systematic research in this field began two decades ago with mixed results but as computer technology matures so does e-Therapy. Each year more studies are published, extending the application of e-Therapy to different populations, disorders and clinical settings. The potential ability to deliver more psychological care to those who need it (and who otherwise might not be able to receive it), to extend the efficiency of scarce clinical resources and to improve monitoring of outcomes presents a great opportunity as we look to the future (Wright *et al.,* 1997).

The challenges in evaluating and employing computer programs clinically cannot be understated. Currently, the vast majority of e-Therapy programs has been developed for adults and more work is needed to find the most suitable and engaging ways to do this for children and adolescents. One of the first empirically evaluated interventions was a CBT program for adults with depression (Selmi et al, 1990), which demonstrated that the computer-delivered therapy was as effective as therapist-delivered CBT in a small trial.

The first e-Therapy programs were really simple and predominately text-based, they essentially involved presenting written text describing self-help strategies to be read off the screen. Interactivity

was limited to multi-choice questions; but as the technology matured the programs have become increasingly more sophisticated (Iluyemi et al, 2012). The new wave of e-Therapy programs allows for greater interactivity, relies more heavily on multimedia (voice, video, animation), incorporates automated emails and text messages (SMS) to enhance adherence or augment the content (Iluyemi et al, 2012). One of the most recent developments is 'gamification' or the convergence of 'serious games' (games designed for a primary purpose other than pure entertainment) with e-Health and e-Therapy. While computer games have received some negative attention, particularly around suggestions that violent video/computer games may cause an increase in aggression, the potential of computer games applied to learning is enormous and, in particular, it is thought that serious games can make a positive contribution (Connolly et al, 2012). An example of a serious e-Health game is Re-Mission, which was shown to improve behavioral outcomes for young patients.

2.1.4 Artificial intelligence in medicine

The advancement in computer technology has encouraged the researchers to develop software for assisting doctors in making decision without consulting the specialists directly (Shapiro, 1992). The software development exploits the potential of human intelligence such as reasoning, making decision, learning (by experiencing) and many others. Artificial intelligence is not a new concept, yet it has been accepted as a new technology in computer science. It has been applied in many areas such as education, business, medical and manufacturing (Shapiro, 1992).

Computer technology could be used to reduce the number of mortality and reduce the waiting time to see the specialist. Computer program or software developed by emulating human intelligence could be used to assist the doctors in making decision without consulting the specialists directly (Shapiro, 1992). The software was not meant to replace the specialist or doctor, yet it was developed to assist general practitioner and specialist in diagnosing and predicting patient's condition from certain rules or experience. Patient with high-risk factors or symptoms or predicted to be highly effected with certain

diseases or illness, could be short listed to see the specialist for further treatment. Employing the technology especially Artificial Intelligence (AI) techniques in medical applications could reduce the cost, time, human expertise and medical error (Iluyemi *et al.,* 2012).

The last two decades have seen a surge in the interest in medical AI. Modern medicine is faced with the challenge of acquiring, analyzing and applying the large amount of knowledge necessary to solve complex clinical problems. The development of medical artificial intelligence has been related to the development of AI programs intended to help the clinician in the formulation of a diagnosis, the making of therapeutic decisions and the prediction of outcome. They are designed to support healthcare workers in their everyday duties, assisting with tasks that rely on the manipulation of data and knowledge. Such systems include artificial neural networks (ANNs), fuzzy expert systems and hybrid intelligent systems (Iluyemi et al, 2012).

2.2 Anatomy of the Human Eye

The eye is a special sense organ made up of three coats/tunics (Remington, 2012): the outer fibrous layer of connective tissue forms the cornea and sclera; the middle vascular layer is composed of the iris, ciliary body and choroid; and the inner layers the retina. Figure 2.1 presents an illustration of some components of the eye, including: iris, pupil, lens, cornea, posterior chamber, choroid, sclera, retina, macula, fovea, optic disk, optic nerve and retinal vessels, which are all described subsequently.

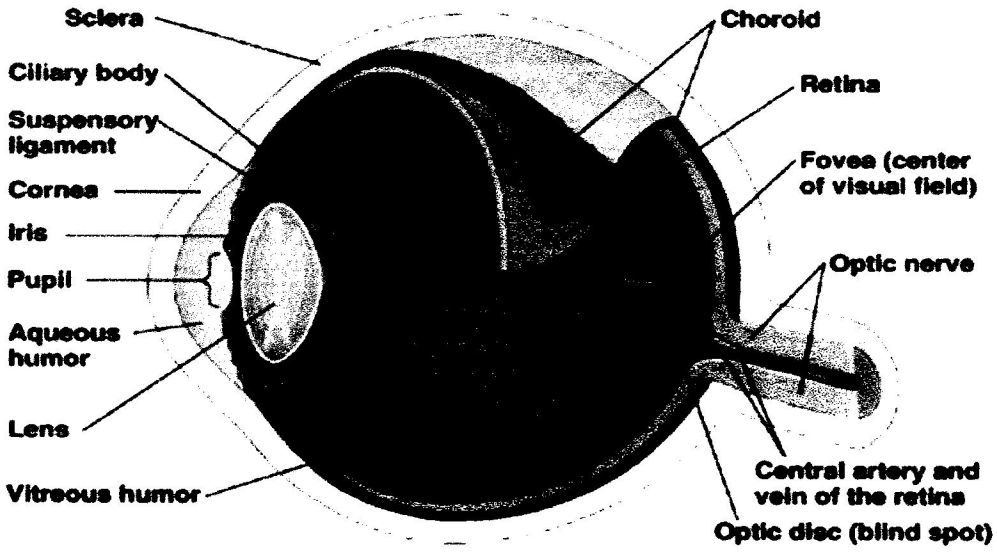

Fig. 2.1: Illustration of components of the anatomy eye (Remington, 2012).

Sclera: The sclera is a membrane of tendon in the eye, also known as the opaque white of the eye. It is covered by the transparent conjunctiva and is composed by two main layers: the lamina fusca, and the episcleral layer anteriorly (which consists of dense vascular connective tissue) (Heath, 2006). Because of its resistance and its robustness, the main task of the sclera is the protection of the inner and consequently, more sensitive parts of the eye, like the retina and choroidea. Its thickness is about $7{,}62\times10^{-4}$m, but in the local where the eye muscles append has a depth more or less of $2{,}54\times10^{-4}$ m. Sclera also contains an elastic tissue denominated of episclera, in its top. This is the blood vessels that nourish the sclera with oxygen and nutrients are located. These vessels are thus visible on the surface of the white of the eye (Heath, 2006).

Choroidea/Choroid: The choroidea is also an association of vessels that nourish the retina with oxygen and nutrients, that its located within the sclera (Clark, 2005). The choroid supplies the overlying retina to a depth of about 130 micrometers which includes the pigment epithelium layer, the layer of rods and cones, the outer nuclear and plexiform layers, and the whole thickness of the foveal retina.

Proliferative macular degeneration is an eye condition that is directly caused by malfunctioning of blood vessels within this layer (Clark, 2005).

Cornea: The cornea is the transparent structure located in the front of the eye, covering the iris, pupil, and anterior chamber. Its transparency allows the refraction of the light rays entering the globe and helps bring light into focus on the retina. The region in which the transition from cornea to sclera and conjunctiva occurs is the limbus (Remington, 2012). Although the cornea is clear and seems to lack substance, it is actually a highly organized group of cells and proteins. But, unlike other tissues it does not contain blood vessels (which will interfere in the process of refraction of light), so it is nourished with oxygen and nutrients through eye fluid and not through blood vessels (that also explains why the cornea is so clear). The corneal tissue is arranged in five basic layers: epithelium, bowman's layer, stroma, Descemete's membrane and endothelium (Heath, 2006).

Retina: The retina refers to the light sensitive tissue in the back of the eyeball. This neural tissue by complex biochemical processes can change light energy into a signal that is transmitted along a neural pathway. The signal passes through the retina, exits the eye through the optic nerve, and is transmitted to various parts of the brain for processing. The retina contains two kinds of light receptors (photoreceptors): the cones and the rods. There are approximately 5 million cones and 100 million rods in each eye. The cones, which are color sensitive, are located in the center of the retina and mainly absorb stronger light. The rods are located peripheral to the fovea and are very sensitive light detectors, absorbing softer light in black and white with the capacity to generate a detectable photocurrent response when they absorb a single photon of light (Heath, 2006). The positions of these two types of photoreceptors differ in many ways across the retina. Usually, the relative densities of cone and rod photoreceptors vary across the retina. The rods initiate vision under low illumination levels, called scotopic light levels, while the cones initiate vision under higher, photopic light levels. The range of

intensities in which both rods and cones can initiate vision is called mesopic intensity levels (Wandell, 2014).

Lens: The crystalline lens is a multilayered structure located in the area of the posterior chamber and provides additional refractive power for accurately focusing images onto the retina (Heath, 2006). In other words, it is the lens that enables the change of focus according to different distances, so that the individual can perceive the object clearly and sharply. The lens is attached to a mass called zonula which is attached to the ciliary body. When a person wants to focus on a near object, a muscle in the ciliary body retracts, allowing the change of shape by the lens, a process called "accommodation". This way the zonula "threads" can loosen up, allowing the lens to contract in diameter and thicken, thus increasing its acuity. As a person becomes older, the flexibility of the lens decreases and vision can become blurry, resulting in a condition named cataracts. It can result in complete removal and replacement of the lens by an artificial one (not capable of accommodation) (Heath, 2006).

Vitreous Body/Humor: The vitreous body is a transparent gel-like substance, made up of small fibers and water in the posterior segment of the eye, behind the lens, that fills the space in front of the lens. The main functions of the vitreous are to transmit light to the retina, and to exercise enough pressure to keep the retinal layers tightly pressed together. This pressure helps maintain the round shape of the eye so the lens can focus sharp images on the retina (Clark, 2005). Beyond the formation of vitreous at birth, when a person is aging the vitreous body shrinks in volume. When the vitreous body decreases in size it can detach from the retina (named vitreous detachment). After passing through the cornea, aqueous humor and lens (anterior segment of the eye), light finally enters in the vitreous. This fluid is not replaced but remains throughout life. A thinner fluid, much like aqueous humor, is added to it and leaves by diffusing through the retina (Clark, 2005).

Fovea: The fovea is the most central part of the macula. The visual cells located in the fovea are packed tightest, resulting in a region with optimal sharpness of vision. The fovea contains no rods, but it does contain a high concentration of cones, approximately 50,000 (Wandell, 2014).

Optic Disc: Also known as the optic nerve head or the blind spot, the optic disc has an oval shape with approximately 1.5 mm diameter and is where the optic nerve attaches to the eye. It is the entry point into the eye for major blood vessels that serve the retina. Only can be seen in the back of the eye with an ophthalmoscope (Wandell, 2014). The absence of visual cells (photoreceptors, i.e., rods or cones) in the optic disc causes the appearance of a blind spot in the field of vision, not existing any image detection in this area. The blind spot of the right eye is located to the right of the centre of vision and vice versa in the left eye. Clinical evaluation of the optic nerve head is critical in the diagnosis and monitoring of glaucoma and other optic neuropathies that may lead to vision loss.

Optic nerve: The optic nerve also known as cranial nerve II, transmits visual information from the retina to the brain, where the signals are interpreted into images. The optic nerve consists of about 1,000,000 nerve threads. The optic nerves from both eyes are reconnected behind the eyes so that everything that is seen in the right field of vision is sent to the left cerebral hemisphere and vice versa (Clark, 2005).

Pupil: The pupil is considered a black hole in the iris, and it is black because the layer of pigment inside the eye absorbs major parts of the light, resulting in a darker shade. However, when pupils appear red in photos it is actually the color of the retina that is reflected. During the visual process the eye must continuously compensate for changes from light to dark and from near to far, so light-dark adaptation is achieved by dilation or contraction of the pupil, whereas near-far adaptation requires a change in the curvature of the lens (accommodation), a change in the lines of sight (convergence), and a change in pupillary width (Heath, 2006). For example, for focusing on near objects, the pupil

decreases in diameter, but it will expand when focusing on distant objects, because a smaller pupil enables better focal depth.

Iris: The iris is the most anterior structure that regulates the amount of light that enters in the pupil, a hole through which the light enters the eye, as previously referred. It has two muscles that control the shape and diameter of the pupil and that are controlled by the autonomous nervous system. In bright light, the iris constricts the pupil, effectively admitting less light. In dim light, the iris dilates the pupil to admit more of the available light. This is a reflex action (Clark, 2005).

2.3 Human Eye Diseases

There are many human eye diseases that can affect vision or lead to blindness. Early diagnosis and treatment are critical to maintaining the health of the eye. A review of some of the common diseases that affects the human eye is done in this section. These diseases include cataract, glaucoma, diabetic retinopathy, age related macula degeneration (ARMD) and retinoblastoma.

2.3.1 Cataract

According to WHO (2014), cataract is responsible for about 51% of blindness all over the world. Cataract is any opacity of the lens, whether it is a small local opacity or a diffuse general loss of transparency (Maltry *et al*, 2012). In other words, a cataract is an opacification of the lens that leads to measurably decreased visual acuity and/or some functional disability as perceived by the patient. The eye's natural crystalline lens helps us focus on people and things at varying distances. Unfortunately, as we grow older this lens often stiffens and hardens, and without its youthful suppleness it loses its ability to focus, creating vision problems (Maltry *et al*, 2012). This condition — for most, a natural consequence of aging — is called presbyopia. And this presbyopia condition in turn leads to the development of cataracts (or a loss in the clarity of lens).

Cataracts may occur as a result of aging or secondary to hereditary factors, trauma, inflammation, metabolic or nutritional disorders, or radiation; however, age-related cataracts are the most common (Maltry *et al*, 2012). At first, in cataracts, symptoms may be undetectable or very slight, however, with time, noticeable changes begin to take place. Common symptoms of cataracts include: Cloudy or blurred vision; Sensitivity to light and glare; Frequent prescription changes for glasses or contact lenses; Poor night vision; Color vision changes and dimming; Double vision in a single eye (Maltry *et al*, 2012).

Fig. 2.2: Fundus image of a cataract-infected eye (Maltry *et al*, 2012).

2.3.2 Glaucoma

Glaucoma is one of the major causes of blindness in the world (WHO, 2014). It is due to the increase in intra ocular pressure within the eyes. The early detection and diagnosis of glaucoma is very important. Glaucoma is a condition that causes damage to the eye's optic nerve and gets worse over time. It is often associated with a buildup of pressure inside the eye. Glaucoma tends to be inherited and may not show up until later in life (WHO, 2014). High amount of intra-ocular pressure (IOP) is one of the major danger components of glaucoma disease. Accusative of present medicament access is to reduce (IOP) inside eyes to prevent structural anthropology damage (Garaci *et al.*, 2009). The increased pressure, called intraocular pressure, can damage the optic nerve, which transmits images to the brain. If damage to the optic nerve from high eye pressure continues, glaucoma will cause

permanent loss of vision. Without early detection and treatment, glaucoma can cause total permanent blindness within a few years (Garaci *et al.*, 2009).

There are two main types of glaucoma: Open-angle glaucoma and Angle-closure glaucoma. Open-angle glaucoma, also called wide-angle glaucoma, is the most common type of glaucoma. The structures of the eye appear normal, but fluid in the eye does not flow properly through the drain of the eye, called the trabecular meshwork (Pooja & Girish, 2016). While angle-closure glaucoma, also called acute or chronic angle-closure or narrow-angle glaucoma, is less common. Poor drainage is caused because the angle between the iris and the cornea is too narrow and is physically blocked by the iris (Pooja & Girish, 2016). Common symptoms of cataracts include: Blurred vision, Severe eye pain, Headache, Rainbow haloes, Nausea and vomiting. There are various approaches available for glaucoma diagnosis among which cup-to-disc ratio (CDR) measurement is one. CDR measurement is a major essential psychological arguments for early diagnosis of glaucoma (Narasimhan, 2011). Depending upon the size and shape of optic disc boundary, it is possible to detect glaucoma. Once optic disc has been identified, other regions of retinal images like fovea and macula can be easily determined (Duanggate *et al.*, 2011).Glaucoma can be derogated by proper treatment and early detection in fundus images (Muramatsu, 2011).

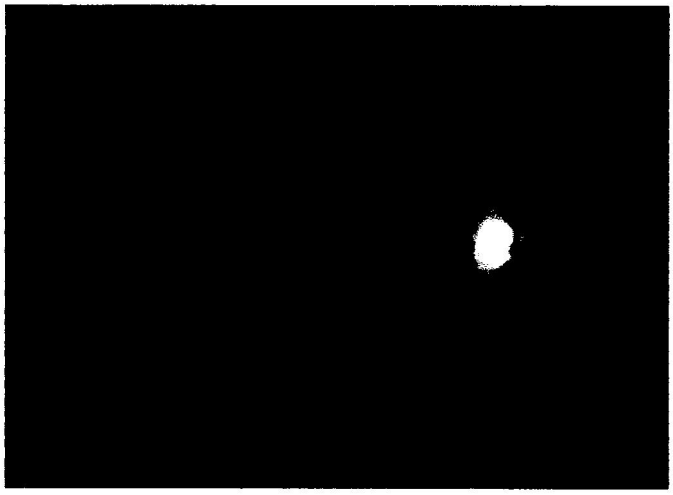

Fig. 2.3. Fundus image of a glaucoma-infected eye (Budai et al., 2013).

2.3.4 Age Related Macula Degeneration

Age Related Macula Degeneration is the third most important cause of blindness across the world, with an estimate of about 196 million people as current victims (WHO, 2014). Age-related macular degeneration, or AMD, is a condition that affects the center of the retina, called the macula. The macula is the part of the eye responsible for our most acute vision, which we use when reading, driving, and performing other activities that require fine, sharp, or straight-ahead vision (Balasundari *et al.,* 2016).

There are two different types of AMD: Dry macular degeneration and wet macular degeneration (Balasundari *et al.,* 2016). In dry macular degeneration, small yellow deposits, known as drusen, accumulate under the macula. Eventually, these deposits are disruptive to vision cells, causing them to slowly break down. With less of the macula working, this causes a gradual loss of central vision as time goes on. This is the most common form of AMD, affecting approximately 90% of people who have the disease (WHO, 2014). In wet macular degeneration, new blood vessels start to grow in areas of the macula where they shouldn't be. This causes rapid damage to the macula that can lead to the loss of central vision in a short period of time. Although this type of AMD affects only about 10% of people with the disease, it is responsible for 90% of severe vision loss associated with AMD (WHO, 2014).

In the early stages, AMD goes largely unnoticed, and can only be detected through a dilated eye exam or automated detection using classifiers such as ANN by automatically analyzing fundus images for detection of the yellow spots on the retina (caused by drusens), which may reveal drusen accumulation (Balasundari *et al.,* 2016). However, as AMD progresses, drusen impair the transportation of vital nutrients to the macula and damages the light-sensitive cells of the retina causing noticeable symptoms, including Blurred vision, dark or empty area in the central area of vision and Distortion of straight lines (Balasundari *et al.,* 2016).

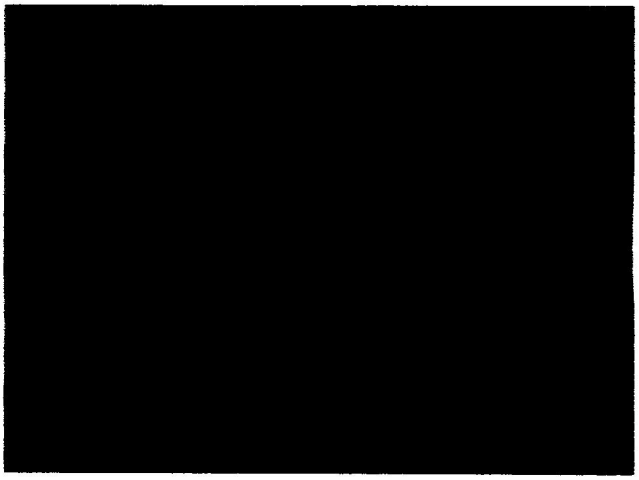

Fig. 2.5. Fundus image of a AMD-infected eye, (Balasundari et al., 2016)

2.3.5 Retinoblastoma

Retinoblastoma is a rare type of eye cancer that usually develops in early childhood, typically before the age of 5. This form of cancer develops in the retina, which is the specialized light-sensitive tissue at the back of the eye that detects light and color (Balasundari *et al.,* 2016). Most children who are diagnosed with retinoblastoma are younger than 5 years old. Retinoblastoma makes up 2% of all cancers diagnosed in children before the age of 15. Generally, 3 out of 4 children have the disease in one eye, while 1 in 4 children have the disease in both eyes (ACS, 2017).

The most common first sign of retinoblastoma is a visible whiteness in the pupil called "cat's eye reflex" or leukocoria (ACS, 2017). This unusual whiteness is particularly noticeable in photographs taken with a flash. Other signs and symptoms of retinoblastoma include crossed eyes or eyes that do not point in the same direction (strabismus); persistent eye pain, redness, or irritation; and blindness or poor vision in the affected eye(s) (ACS, 2017). Retinoblastoma is often curable when it is diagnosed early, either through a physical ophthalmology exam or via automated detection by analyzing fundus images using a classifier algorithm (Balasundari *et al.,* 2016). However, if it is not treated promptly, this cancer can spread beyond the eye to other parts of the body. This advanced form of retinoblastoma can be life-threatening.

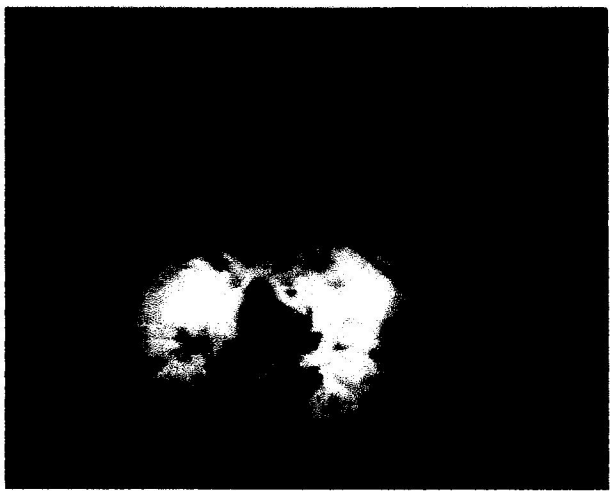

Fig. 2.6. Fundus image of a retinoblastoma-infected eye (Balasundari et al., 2016)

2.4 Eye Image Acquisition

Before any video or image processing can commence an image must be captured by a camera and converted into a manageable entity. This is the process known as image acquisition. There are various techniques used in image acquisition, based on how severe the disease being diagnosed may be. Few of them will be considered in this section including fundus imaging, hyperspectral imaging and scanning laser ophthalmoscopy.

2.4.1 Fundus Imaging

Fundus imaging is the process whereby a 2-D representation of the 3-D retinal semitransparent tissues projected onto the imaging plane is obtained using reflected light. Thus, any process which results in a 2-D image, where the image intensities represent the amount of a reflected quantity of light, is fundus imaging (Usher *et al.,* 2003). In fundus imaging, image intensities represent the amount of reflected light of a specific waveband, therefore examinations are simply performed by viewing the fundus of eyes using the natural way of the light: light is directed through the pupil to the retina and the fundus with its normal and abnormal parts can be observed from the reflected light. Usually, the best fundus images are obtained when the eye is well dilated, fixation is on the target; and lids and lashes are held wide open (Usher *et al.,* 2003).

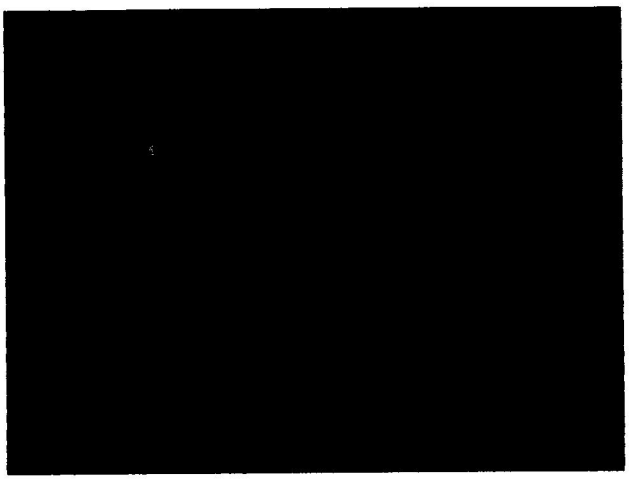

Fig. 2.7. Fundus image of a normal eye (Usher et al., 2003)

2.4.2 Hyperspectral imaging

Image intensities represent the amount of reflected light of multiple specific wavelength bands. Hyperspectral images contain a wealth of data. Hyperspectral imaging of the human retina is a relatively new concept that has the potential to determine the metabolic status of the retina (Usher *et al.*, 2003). The hyperspectral technique allows wavelength-specific visualization of retinal lesions that may be subvisible using a white light source camera. This hyperspectral technique may facilitate localization of retinal and disc pathology and consequently facilitate the diagnosis and management of common retinal diseases such as diabetic retinopathy and cataracts (Walter *et al.*, 2002). Hyperspectral deals with imaging narrow spectral bands over a continuous spectral range, and produce the spectra of all pixels in the scene. Hyperspectral images are usually produced by instruments called imaging spectrometers (Walter *et al.*, 2002). Spectroscopy is the study of light that is emitted by or reflected from materials and its variation in energy with wavelength (Usher *et al.*, 2003. Reflectance varies with wavelength for most materials because energy at certain wavelengths is scattered or absorbed to different degrees. Hyperspectral imaging is capable of detecting oximetric changes in the retina and monitoring its response to treatment (Usher *et al.*, 2003).

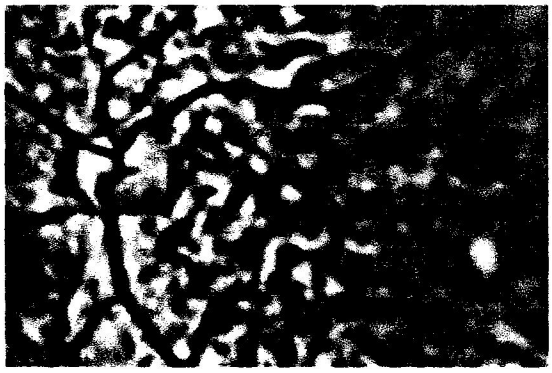

Fig. 2.8. Hyperspectral imaging (Usher et al., 2003)

2.4.3 Scanning laser ophthalmoscopy (SLO)

Image intensities represent the amount of reflected single wavelength laser light obtained in a time sequence. SLO utilizes horizontal and vertical scanning mirrors to scan a specific region of the retina and create raster images viewable on a television monitor (Sinthanayothin *et al.*, 2003). While it is able to image the retina in real time, it has issues with reflections from eye astigmatism and the cornea. Eye movements additionally can confound the data from SLO Unlike conventional photography, which obtains two-dimensional imaging. Scanning laser techniques utilize confocal imaging methods to obtain high resolution images both perpendicular (x-axis, y-axis) to optic axis and along the optic axis (z-axis). The Heidelberg Retina Tomograph II (HRT II) represents the latest iteration in the application of confocal scanning laser ophthalmoscopy to the examination of the optic disc. The HRT II is a scanning laser ophthalmoscope specifically designed to acquire three-dimensional images of the optic nerve head and posterior pole (Sinthanayothin *et al.*, 2003).

The intensity of the scanning diode laser is 100 times lower than the luminance of a digital fundus flash camera, making the imaging process much more comfortable to the patient than with conventional fundus photography (Sinthanayothin *et al.*, 2003). As a method used to image the retina with a high degree of spatial sensitivity, it is helpful in the diagnosis of glaucoma, macular degeneration, and other

retinal disorders. Lateral resolution from SLO has been the ability to determine the spatial distribution of cone cells around the fovea. The imaging of Retinal Pigment Epithelium optic nerve head and posterior pole. It has greater translational resolution (Sinthanayothin *et al.*, 2003).

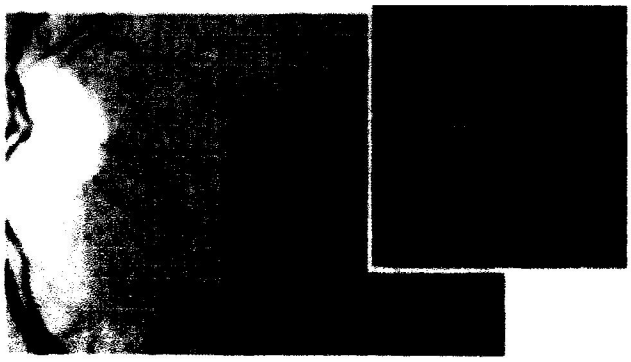

Fig 2.9: Scanning laser Ophthalmology (Usher et al., 2003)

2.5 Image Pre-Processing Techniques

With great improvement in field of medical imaging, Image processing technique helps in early diagnosis of glaucoma, diabetic retinopathy and other eye disease. Retinal fundus images assist trained clinicians to diagnose any abnormality and any change in retina. These images are captured by using special devices called ophthalmoscopes. Medical image analysis and processing has great significance in non-invasive treatment and clinical study. There are several techniques used in Image processing, however, few of them will be considered in this section including gray scale conversion, thresholding, adaptive histogram equalization, morphological operations and Gaussian filter.

2.5.1 Gray-scale conversion

Gray scale conversion is one of the simplest enhancement techniques used in image preprocessing. A grayscale digital image is an image in which the value of each pixel is a single sample, that is, it carries only intensity information. Images of this sort, also known as black-and-white, are composed exclusively of shades of gray, varying from black at the weakest intensity to white at the strongest (Johnson, 2006). In many of the computer vision applications, color-to-grayscale conversion

algorithms are required to preserve the salient features of the color images, such as brightness, contrast and structure of the color image.

Grayscale images are distinct from one-bit bi-tonal black-and-white images, which in the context of computer imaging are images with only two colors, black and white (also called bilevel or binary images). Grayscale images have many shades of gray in between. Grayscale images are often the result of measuring the intensity of light at each pixel in a single band of the electromagnetic spectrum (e.g. infrared, visible light, ultraviolet, etc.), and in such cases they are monochromatic proper when only a given frequency is captured, but also they can be synthesized from a full color image (Johnson, 2006).

Furthermore, gray-scale conversion often leads to a process called binarization in image pre-processing. Binarization is the process of converting a pixel image into a binary image. A binary image is a digital image that has only two possible values for each pixel (Schmid & Mohr, 1997). Typically, the two colors used for a binary image are black and white, though any two colors can be used. The color used for the object(s) in the image is the foreground color while the rest of the image is the background color. In the document-scanning industry, this is often referred to as "bi-tonal" (Schmid & Mohr, 1997). Binary images are also called bi-level or two-level. This means that each pixel is stored as a single bit—i.e., a 0 or 1. The names black-and-white, B&W, monochrome or monochromatic are often used for this concept, but may also designate any images that have only one sample per pixel, such as grayscale images. Figure 2.10 shows the graphical description of fundus image before and after grayscale preprocessing.

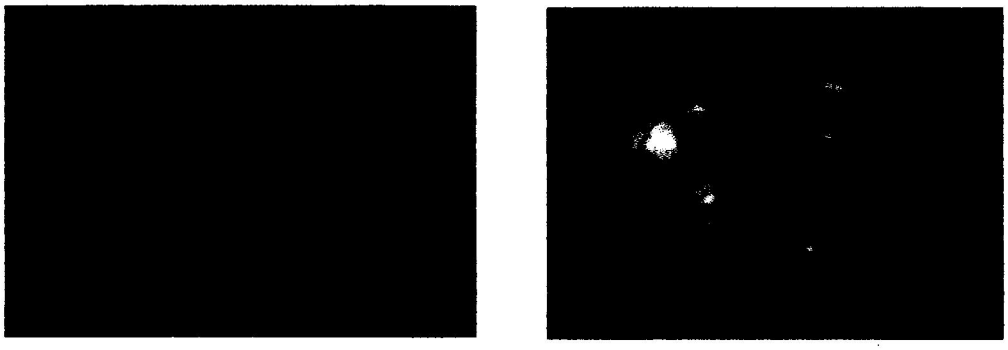

Fig. 2.10. Fundus image before and after grayscaling (Schmid & Mohr, 1997)

2.5.2 Thresholding

Thresholding is a simple processing technique, where the images could be viewed as the result of trying to separate the eye from the background (Schmid & Mohr, 1997). Thresholding is a method of producing regions of uniformity within an image based on some threshold criterion. Thresholding is the simplest method of image segmentation. From a grayscale image, thresholding can be used to create binary images (Schmid & Mohr, 1997). The simplest thresholding methods replace each pixel in an image with a black pixel if the image intensity is less than some fixed constant, or a white pixel if the image intensity is greater than that constant. In the example image on the right, this results in the dark tree becoming completely black, and the white snow becoming completely white.

To make thresholding completely automated, it is necessary for the computer to automatically select the threshold T. Schmid & Mohr (1997) categorize thresholding methods into six groups based on the information the algorithm manipulates; Histogram shape-based methods, where, for example, the peaks, valleys and curvatures of the smoothed histogram are analyzed; clustering-based methods, where the gray-level samples are clustered in two parts as background and foreground (object), or alternately are modeled as a mixture of two Gaussians; entropy-based methods result in algorithms that use the entropy of the foreground and background regions, the cross-entropy between the original and binarized image; object Attribute-based methods search a measure of similarity between the gray-level

and the binarized images, such as fuzzy shape similarity, edge coincidence; spatial methods [that] use higher-order probability distribution and/or correlation between pixels; local methods adapt the threshold value on each pixel to the local image characteristics. In these methods, a different T is selected for each pixel in the image.

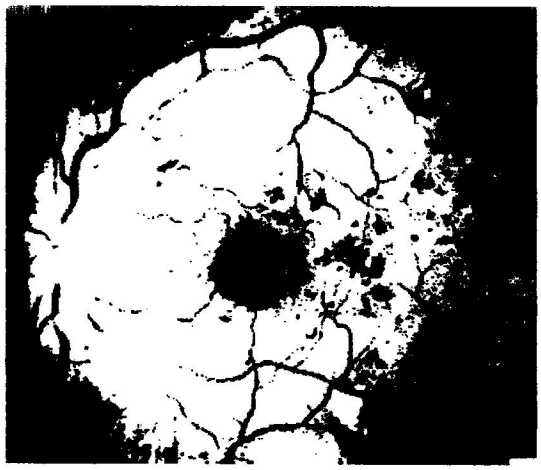

Fig. 2.11. A fundus image after thresholding (Schmid & Mohr, 1997)

2.5.3 Adaptive Histogram Equalization

Adaptive Histogram equalization is a method in digital image processing that is used to enhance the contrast of the image (Sund & Moystad, 2006). Adaptive histogram operates on different parts of the image and uses them to reallocate the lightness value of the image. Due to this, even local lower contrast area gains a higher contrast. This is also called contrast limited adaptive histogram equalization. It is a computer image processing technique used to improve contrast in images. It differs from ordinary histogram equalization in the respect that the adaptive method computes several histograms, each corresponding to a distinct section of the image, and uses them to redistribute the lightness values of the image. It is therefore suitable for improving the local contrast and enhancing the definitions of edges in each region of an image (Sund & Moystad, 2006).

However, AHE has a tendency to over-amplify noise in relatively homogeneous regions of an image. A variant of adaptive histogram equalization called contrast limited adaptive histogram equalization (CLAHE) prevents this by limiting the amplification (Sund & Moystad, 2006). Ordinary histogram equalization uses the same transformation derived from the image histogram to transform all pixels. This works well when the distribution of pixel values is similar throughout the image. However, when the image contains regions that are significantly lighter or darker than most of the image, the contrast in those regions will not be sufficiently enhanced. Adaptive histogram equalization (AHE) improves on this by transforming each pixel with a transformation function derived from a neighborhood region. It was first developed in the year 1974 for use in aircraft cockpit displays (Ketcham *et al.*, 1974).

Fig. 2.12. Contrast enhancement of fundus images by adaptive histogram equalization (Sund & Moystad, 2006)

2.5.4 Gaussian filter

In image processing, a Gaussian filter (also known as Gaussian smoothing) is the result of blurring an image by a Gaussian function. It is a widely used effect in graphics software, typically to reduce image noise and reduce detail (Singh & Kaur, 2012). The visual effect of this blurring technique is a smooth blur resembling that of viewing the image through a translucent screen, distinctly different from the bokeh effect produced by an out-of-focus lens or the shadow of an object under usual illumination.

Gaussian smoothing is also used as a pre-processing stage in computer vision algorithms in order to enhance image structures at different scales (Singh & Kaur, 2012).

Mathematically, applying a Gaussian blur to an image is the same as convolving the image with a Gaussian function. This is also known as a two-dimensional Weier-strass transform. By contrast, convolving by a circle (i.e., a circular box blur) would more accurately reproduce the bokeh effect. Since the Fourier transform of a Gaussian is another Gaussian, applying a Gaussian blur has the effect of reducing the image's high-frequency components; a Gaussian blur is thus a low pass filter (Singh & Kaur, 2012).

Gaussian blurring is commonly used when reducing the size of an image. When down-sampling an image, it is common to apply a low-pass filter to the image prior to resampling. This is to ensure that spurious high-frequency information does not appear in the down-sampled image (aliasing). Gaussian blurs have nice properties, such as having no sharp edges, and thus do not introduce ringing into the filtered image (Singh & Kaur, 2012).

Fig. 2.13. Smoothing of fundus images by applying Gaussian filter (Singh & Kaur, 2012).

2.5.5 Morphological Operations

Binary images may contain numerous imperfections. In particular, the binary regions produced by simple thresholding are distorted by noise and texture (Sarkar & Leong, 2001). Morphological image processing pursues the goals of removing these imperfections by accounting for the form and structure of the image. These techniques can be extended to greyscale images. Morphological image processing is a collection of non-linear operations related to the shape or morphology of features in an image. Morphological operations rely only on the relative ordering of pixel values, not on their numerical values, and therefore are especially suited to the processing of binary images. Morphological operations can also be applied to greyscale images such that their light transfer functions are unknown and therefore their absolute pixel values are of no or minor interest.

Morphology is a broad set of image processing operations that process images based on shapes (Sarkar & Leong, 2001). Morphological operations apply a structuring element to an input image, creating an output image of the same size. In a morphological operation, the value of each pixel in the output image is based on a comparison of the corresponding pixel in the input image with its neighbors. By choosing the size and shape of the neighborhood, one can construct a morphological operation that is sensitive to specific shapes in the input image. In morphological operations, while some operations test whether the element "fits" within the neighborhood, others test whether it "hits" or intersects the neighborhood (Sarkar & Leong, 2001).

The most basic morphological operations are dilation and erosion (Sarkar & Leong, 2001). Dilation adds pixels to the boundaries of objects in an image, while erosion removes pixels on object boundaries. The number of pixels added or removed from the objects in an image depends on the size and shape of the structuring element used to process the image. In the morphological dilation and erosion operations, the state of any given pixel in the output image is determined by applying a rule to the corresponding

pixel and its neighbors in the input image. The rule used to process the pixels defines the operation as a dilation or an erosion.

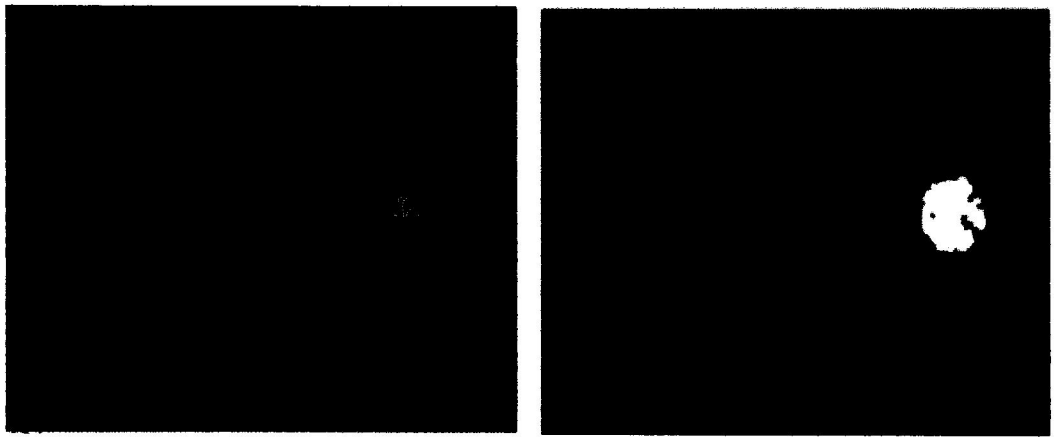

Fig. 2.14. Fundus image, before and after dilation and erosion (Sarkar & Leong, 2001).

2.6 Feature Extraction

Feature plays a very important role in the area of image processing. Before getting features, various image preprocessing techniques like gray-scale conversion, adaptive histogram equalization, thresholding etc. are applied on the sampled image. After that, feature extraction techniques are applied to get features that will be useful in classifying and recognition of images. Feature extraction techniques are helpful in various image processing applications e.g. character recognition. As features define the behavior of an image, they show its place in terms of storage taken, efficiency in classification and obviously in time consumption also.

Mostly, Feature extraction algorithms used to detect and isolate various segment of a medical image. Nowadays more research in medical image processing which makes feature extraction and detection of important metadata in large number of image series (Harisha, 2015). However, the process of extracting important features from large image datasets of medical images is extremely demanding in terms of computation time, storage capacity and network bandwidth. The Map Reduce framework is a

distributed computing framework, which can be recently been used for large–scale image description and analysis (Harisha, 2015). In this section, a review of three feature extraction techniques is done including Gray-level Co-occurrence matrix (GLCM), Principal Component Analysis (PCA) and Gabor filter.

2.6.1 Gray-level Co-occurrence matrix (GLCM)

GLCM is a statistical method of examining the textures of images by considering the spatial relationship of the pixels (Abdullahi *et al.,* 2014). Gray Level Co-occurrence Matrix (GLCM) assesses image properties associated to Second-Order statistics. Zulpe et al (2012) shows that the number of gray level 'G' of an image is represented by the row and column of GLCM and the element used by the matrix is given as:

$$(i,j|\Delta x,\Delta y) \ \ and \ (i,|d,\theta) \tag{2.1}$$

Where in the first expression of equation above, $p(i,j)$ represent the frequency of the matrix element separated by the distance $\Delta x,\Delta y$ and the second expression represents the second order probability values for changes between gray levels i and j at a distance d and angleθ.

Most features in medical images are all functions of angle and distance and using only horizontal or diagonal offset may not be a better representation of the entire image (Abdullahi *et al.,* 2014). Several features can be extracted from GLCM which are used to train classifiers whose performance depends on the extracted features. Some features that can be extracted from GLCM as given by Zulpe et al (2012) includes Contrast, Correlation, Energy and Homogeneity.

Contrast: This is the measure of the intensity contrast between a pixel and its neighbor over the whole image.

$$contrast = \sum_{n=0}^{G-1} n^2 \left\{ \sum_{i=0}^{G-1} \sum_{j=0}^{G-1} P(i,j) \right\}, |i-j| \tag{2.2}$$

Correlation: Returns a measure of how correlated a pixel is to its neighbor over the whole image. Correlation is 1 or -1 for a perfectly positively or negatively correlated image.

$$Correlation = \sum_{i,j} \frac{(i-\mu i)(j-\mu j)p(i,j)}{\sigma_i \sigma_j} \quad (2.3)$$

Energy: Energy is the property which returns the sum of squared elements for an input image, in the GLCM. For a constant image, the energy value is ideally "1".

$$Energy = \sum_{i,j} p(i,j)^2 \quad (2.4)$$

Homogeneity: Homogeneity is the property which returns a value that measures the closeness of the distribution of elements in the GLCM to the GLCM diagonal. Homogeneity is 1 for a diagonal GLCM.

$$Homogeneity = \sum_{i,j} \frac{p(i,j)}{1+|i-j|} \quad (2.5)$$

GLCM feature extraction has been applied successfully for most diagnostic systems and performs significantly better than principal component analysis (PCA) feature extraction technique (Singh & Kaur, 2012).

2.6.2 Gabor filter

In image processing, a Gabor filter, named after Dennis Gabor, is a linear filter used for edge detection (Henriksen, 2007). Frequency and orientation representations of Gabor filters are similar to those of the human visual system, and they have been found to be particularly appropriate for texture representation and discrimination. In the spatial domain, a 2D Gabor filter is a Gaussian kernel function modulated by a sinusoidal plane wave. Simple cells in the visual cortex of mammalian brains can be modeled by Gabor functions. Thus, image analysis with Gabor filters is thought to be similar to perception in the human visual system (Henriksen, 2007).

A set of Gabor filters with different frequencies and orientations may be helpful for extracting useful features from an image (Haghighat *et al.,* 2013). In the discrete domain, two-dimensional Gabor filters are given by:

$$G_c[i,j] = Be^{-\frac{(i^2+j^2)}{2\sigma^2}} \cos(2\pi f(i\cos\theta + j\sin\theta)) \quad (2.6)$$

$$G_s[i,j] = Ce^{-\frac{(i^2+j^2)}{2\sigma^2}} \sin(2\pi f(i\cos\theta + j\sin\theta)) \quad (2.7)$$

Where B and C are normalizing factors to be determined. 2-D Gabor filters have rich applications in image processing, especially in feature extraction for texture analysis and segmentation (Haghighat *et al.,* 2013). **f** defines the frequency being looked for in the texture. By varying θ, we can look for texture oriented in a particular direction. By varying σ, we change the support of the basis or the size of the image region being analyzed.

2.6.3 Principal Component Analysis

Principal Component Analysis (PCA) is a common feature extraction method used in medical image processing (Kumar & Deepashree, 2013). Technically, PCA finds the eigenvectors of a covariance matrix with the highest eigenvalues and then uses those to project the data into a new subspace of equal

or less dimensions. Practically, PCA converts a matrix of m features into a new dataset of n features, usually less than m features. In other words, it reduces the number of features by constructing a new but smaller number variables which capture a significant portion of the information found in the original features (Kumar & Deepashree, 2013).

PCA is a mathematical procedure that uses an orthogonal transformation to convert a set of observations of possibly correlated variables into a set of values of uncorrelated variables called principal components. This procedure includes: center the data X; compute the covariance matrix C; obtain the eigen vectors and eigen values of the covariance matrix U, P; project the original data in the eigenspace – $P = U^T.X$ (Kumar & Deepashree, 2013).

The number of principal components is less than or equal to the number of original variables. This transformation is defined in such a way that the first principal component has as high a variance as possible (that is, accounts for as much of the variability in the data as possible), and each succeeding component in turn has the highest variance possible under the constraint that it be orthogonal to (uncorrelated with) the preceding components. Principal components are guaranteed to be independent only if the data set is jointly normally distributed. PCA is sensitive to the relative scaling of the original variables. Depending on the field of application, it is also named the discrete Karhunen– Loeve transform (KLT), the Hotelling transform or proper orthogonal decomposition (POD)

2.7 Machine Learning Algorithms for Digital Health

On completion of image preprocessing and feature extractions, there is then a need to use a machine learning algorithm that will help give a useful meaning to the extracted features. Such algorithms extract useful information from datasets (e.g., images) to solve important problems in Image Processing and Computer Vision. A review of few machine learning algorithms is done in this section including

K-Nearest Neighborhood Algorithm (KNN), Artificial Neural Network (ANN), Support Vector Machine (SVM), Fuzzy Logic and Hidden Markov Model (HMM).

2.7.1 K-Nearest Neighborhood Algorithm (KNN)

K - Nearest Neighbor is a kind of instance-based learning, where the function is only locally approximated and all computation is referred until classification (Alamelu *et al.*, 2015). This technique is called lazy learning because it does not need any training or minimal training phase. All the training data is needed only during the testing phase and this technique uses all the training data so that if we have a large data set then we need special method to work on part of data which is the algorithmic approach (Alamelu *et al.*, 2015). KNN algorithm has been used in many applications in areas such as data mining, statistical pattern recognition, image processing. Successful applications include recognition of handwriting and satellite image. KNN can be described in 3 steps namely: Classification, binary classification and K-preferably odd to avoid ties.

Although classification is the primary application of KNN, it can also be used for density estimation. The k-nearest neighbor algorithm is one of the simplest algorithm of all machine learning algorithms and its' classification was formulated from the requirement to perform several analysis when reliable parametric estimates of probability densities are not known or difficult to determine (Alamelu *et al.*, 2015). Few of its constraints, however includes: Sensitive to noise and irrelevant features, computationally expensive, large memory requirements, and more frequent classes dominate result.

2.7.2 Artificial Neural Network (ANN)

Artificial neural networks (ANN) consider classification as one of the most dynamic research and application areas. ANN teaches the system to execute task, instead of programming computational system to do definite tasks. Artificial neural networks (ANN) are networks constituted by highly interconnection of artificial neurones that mimic the behavior of the brain in a simplified computational

form (Abdullahi *et al.,* 2014). A neuron is the fundamental information-processing unit of an artificial neural network that consists of a set of synaptic links, an adder and an activation function that receives information, process it mathematically and pass it to other neurons (Tahseen *et al.,* 2011). They are used to perform computations like pattern recognition, pattern matching, classification and forecasting.

ANNs are computational analytical tools which are inspired by the biological nervous system. They consist of networks of highly interconnected computer processors called 'neurons' that are capable of performing parallel computations for data processing and knowledge representation (McCulloch *et al.,* 1943). Their ability to learn from historical examples, analyze non-linear data, handle imprecise information and generalize enabling application of the model to independent data has made them a very attractive analytical tool in the field of medicine. McCulloch and Pitts (1943) invented the first artificial neuron using simple binary threshold functions. The next important milestone came when Frank Rosenblatt, a psychologist, developed the Perceptron in 1958 as a practical model. Many variations of the basic Perceptron network have been proposed but the most popular model has been multilayer feed-forward Perceptron (Rosenblatt, 1958) (See Fig. 2.15). These networks are made up of layers of neurons, typically an input layer, one or more middle or hidden layers and an output layer, each of which are fully connected to other layer.

The neurons in ANN are connected by links, and each link has a numerical weight associated with it. A neural network 'learns' through repeated adjustments of these weights. One of the important characters of ANNs is that they can learn from their experience in a training environment. The use of multilayer feed-forward Perceptron was restricted by the lack of a suitable learning algorithm until Paul Werbos (1974), a PhD student, introduced 'back-propagation' learning (Werbos, 1974). Some of the other popular network designs include Hopfield networks, Radial Basis Function, and the Self-Organizing Feature Map (Tahseen *et al.,* 2011). ANNs have already found a wide variety of applications in the real world. Their ability to classify and recognize patterns accurately has attracted

researchers to apply them in solving many clinical problems. As we realize that diagnosis, treatment and predicting outcome in many clinical situations is dependent on a complex interaction of many clinical, biological and pathological variables there is a growing need for analytical tools like ANNs which can exploit the intricate relationships between these variables (Tahseen *et al.*, 2011)

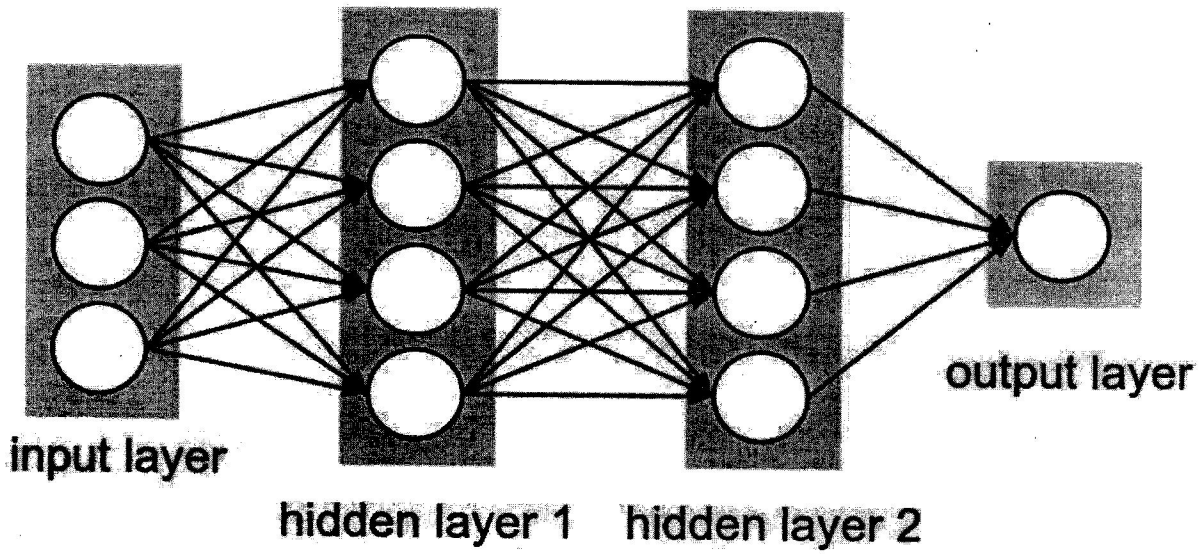

Figure 2.15: A multilayered feed-forward artificial neural network (Tahseen et al. 2011).

Baxt (1990) was one of the first researchers to explore the clinical potentials of ANNs. He developed a neural network model which accurately diagnosed acute myocardial infarction and latter prospectively validated his work with similar accuracy. Since then, ANNs have been applied in almost every field of medicine.

Feed-Forward Neural Network: A feed forward neural network is an artificial neural network wherein connections between the units do not form a cycle. This is different from recurrent neural networks. The feed forward neural network was the first and simplest type of artificial neural network devised. In this network, the information moves in only one direction, forward, from the input nodes, through the hidden nodes (if any) and to the output nodes. There are no cycles or loops in the network (Tahseen *et al,* 2011)

Back Propagation Neural Network: Back propagation is the generalization of the Widrow-Hoff learning rule to multiple-layer networks and nonlinear differentiable transfer functions (Yegnanarayana, 1999). The term back propagation refers to the manner in which the gradient is computed for nonlinear multilayer networks (Sheeba *et al.*, 2009). There are a number of variations on the basic algorithm that are based on other standard optimization techniques, such as conjugate gradient and Newton methods. Properly trained back propagation networks tend to give reasonable answers when presented with inputs that they have never seen. Typically, a new input leads to an output similar to the correct output for input vectors used in training that are similar to the new input being presented. This generalization property makes it possible to train a network on a representative set of input/target pairs and get good results without training the network on all possible input/output pairs. The simplest implementation of back propagation learning updates the network weights and biases in the direction in which the performance function decreases most rapidly, the negative of the gradient (Yegnanarayana, 1999).

2.7.3 Fuzzy Logic

Fuzzy logic is the science of reasoning, thinking and inference that recognizes and uses the real world phenomenon – that everything is a matter of degree. Instead of assuming everything is black and white (conventional logic), fuzzy logic recognizes that in reality, most things would fall somewhere in between; that is varying shades of grey. It was popularized by Lofti Zadeh (1965) an engineer from the University of California (Zadeh, 1965). It uses continuous set membership from 0 to 1 in contrast to Boolean or conventional logic which uses sharp distinctions, i.e. 0 for false and 1 for true. Medicine is essentially a continuous domain and most medical data is inherently imprecise. Fuzzy logic is a data handling methodology that permits ambiguity and hence is particularly suited to medical applications. It captures and uses the concept of fuzziness in a computationally effective manner. Zadeh wrote in

Fuzzy expert systems have the structure of a series of 'if – then' rules for modelling. The techniques of fuzzy logic have been explored in many medical applications. Schneider et al. (2002) showed that fuzzy logic performed better than multiple logistic regression analysis in diagnosing lung cancer using tumour marker profiles. Similarly, the application of fuzzy logic has been explored in the diagnosis of acute leukaemia (Belacel *et al.,* 2001), and breast (Seker *et al.,* 2002) and pancreatic cancer (Halm *et al.,* 2000). They have also been applied to characterize ultrasound images of the breast (Koyama *et al.,* 1997), ultrasound (Badawi *et al.,* 1999) and CT scan (Klein *et al.,* 1996) images of liver lesions and MRI images of brain tumors (Seker *et al.,* 2002). Fuzzy logic has also been used to predict survival in patients with breast cancer (Seker *et al.,* 2002). Fuzzy controllers have been designed for the administration of vasodilators to control blood pressure in the peri-operative period, and also in the administration of anaesthetics in the operating room (Mason *et al.,* 1997)

2.7.4 Support Vector Machines (SVM)

In machine learning, support vector machines (SVMs) are supervised learning models with associated learning algorithms that analyze data used for classification and regression analysis (Alamelu *et al.,* 2015). Given a set of training examples, each marked as belonging to one or the other of two categories, an SVM training algorithm builds a model that assigns new examples to one category or the other, making it a non-probabilistic binary linear classifier. An SVM model is a representation of the examples as points in space, mapped so that the examples of the separate categories are divided by a clear gap that is as wide as possible. New examples are then mapped into that same space and predicted to belong to a category based on which side of the gap they fall (Alamelu *et al.,* 2015).

SVM is a supervised classifier like ANN, it learns statistically based on structural minimization of input vector and mapping it into a high dimensional feature space using a non-linear mapping kernel (Abdullahi *et al.,* 2014). There are two major categories of Support Vector Machines. The first is the hard margin SVM which has the property of linear separability in the feature space and also has the

ability to maximize generalization. On the other hand, the second is the Soft margin SVM, which is not separable in the feature space and has the ability to minimize and maximize classification error simultaneously. In addition to performing linear classification, SVMs can efficiently perform a non-linear classification using what is called the kernel trick, implicitly mapping their inputs into high-dimensional feature spaces. The architecture of SVM can be described in 3 steps (Alamelu *et al.*, 2015): The first step is the formulation for two-class classification problems, the second involves the mapping of the input space into the feature space, while the final step is the determination of the optimal hyperplane in the feature space.

2.7.5 Hidden Markov Model (HMM)

A hidden Markov model (HMM) is a statistical Markov model in which the system being modeled is assumed to be a Markov process with unobserved (hidden) states. An HMM can be presented as the simplest dynamic Bayesian network. The mathematics behind the HMM were developed by L. E. Baum and coworkers (Baum & Petri, 1966). It is closely related to an earlier work on the optimal nonlinear filtering problem by Ruslan L. Stratonovich, (1960) who was the first to describe the forward-backward procedure.

In simpler Markov models (like a Markov chain), the state is directly visible to the observer, and therefore the state transition probabilities are the only parameters. In a hidden Markov model, the state is not directly visible, but the output, dependent on the state, is visible (Boudaren, 2012). Each state has a probability distribution over the possible output tokens. Therefore, the sequence of tokens generated by an HMM gives some information about the sequence of states. The adjective 'hidden' refers to the state sequence through which the model passes, not to the parameters of the model; the model is still referred to as a 'hidden' Markov model even if these parameters are known exactly (Baum & Petri, 1966).

refers to the state sequence through which the model passes, not to the parameters of the model; the model is still referred to as a 'hidden' Markov model even if these parameters are known exactly (Baum & Petri, 1966).

Hidden Markov models are especially known for their application in temporal pattern recognition such as speech, handwriting, gesture recognition, (Starner & Pentland, 1995) part-of-speech tagging, musical score following, (Pardo & Birmingham, 2005) partial discharges and bioinformatics. A hidden Markov model can be considered a generalization of a mixture model where the hidden variables (or latent variables), which control the mixture component to be selected for each observation, are related through a Markov process rather than independent of each other. Recently, hidden Markov models have been generalized to pairwise Markov models and triplet Markov models which allow consideration of more complex data structures (Boudaren, 2012) and the modelling of nonstationary data. (Boudaren, 2012)

2.8 Related Works

Several computing techniques have been proposed for the detection of eye abnormalities and retinal diseases. Usher et.al (2003) described the development of an automated system to detect abnormalities such as microneurysm, haemorrhages and exudates in color retinal images. They used image processing to standardize color and contrast enhancement, segmentation to reveal lesions followed by classification of lesions using neural network. Although a sensitivity of 100% and a mean number of 0.1 false positives per image were obtained, the resulting algorithm was tested using only ten images.

Kevin Noronha (2006) performed a work which uses the enhancement techniques on retinal fundus Image to highlight the features for detection of abnormal eyes. This work specifies the methods used to detect main features of retinal fundus images such as optic disk, fovea, and exudates and blood vessels using different techniques. To determine the optic Disk and its centre, the brightest part of the

fundus were located and hough transform was further applied, obtaining a sensitivity of 92.8% and a positive predictive value of 92.4% in a small dataset of 30 retinal images.

Bock et al (2007) proposed glaucoma classification using image based features. The method is automated, appearance based glaucoma classification system. Segmentation is not used. This is purely data driven approach which is applicable in large scale screening examination. Several types of image based features were analysed and are combined to capture glaucomatous structure. This method does not depend on the explicit outlining of the optic disc. This method gives the success rate of 86%. One limitation of this method is that classification on separate test data and training data shows slightly inferior performance.

L´aszl´o (2009) devised a novel automated glaucoma classification technique, depending on image features from fundus photographs. In this study, data-driven technique does not need any manual assistance. First of all size differences, non-uniform illumination and blood vessels are eliminated from the images. They then extracted the high dimensional feature vectors. Finally compression is done using PCA and the combination before classification with SVMs takes place. The Glaucoma Risk Index produced by the proposed system with a 2-stage SVM classification scheme achieved 86% success rate. This is comparable to the performance of medical experts in detecting glaucomatous eyes from such images. Since Glaucoma Risk Index is computed automatically from fundus images acquired by an inexpensive and widely available camera it is suggested that the system could be used in glaucoma mass screenings.

Furthermore, Vahabi (2010) developed a system which uses an automated approach for detection of Optic Disc from non-dilated retinal images. The Author describes a new filtering approach like Sobel edge detection, Texture Analysis, Intensity and Template matching to detect Optic Disc. The proposed algorithm is applied in wavelet domain on 150 images of Messidor dataset. The algorithm achieved a

sensitivity rate of 88.5% and a positive predictive value of 89.4%, however the time complexity of the system was a drawback.

Stanislav et al (2011) used Gabor filter and tophat transform for segmentation of retinal blood vessel. In this work, the author gave a method for retinal blood vessels segmentation by applying firstly Gabor filter to enhance blood vessels and then applying top-hat transform. Later on, the output is converted to binary image with p-tile thresholding. The evaluations showed that the result produced an impressive sensitivity of 93%, however, a small dataset of 20 images were used in testing.

Ramani (2012) used retinal image analysis and data mining techniques for automatic prediction of diabetic retinopathy and glaucoma. This paper proposed a novel approach for automatic disease detection. Retinal image analysis and data mining techniques are used to accurately categorize the retinal images as either Normal, Diabetic Retinopathy and Glaucoma affected. The technique recorded a sensitivity and accuracy of 93% and 92% respectively.

Chalinee et al (2013) proposed "Image Processing Techniques For Glaucoma Detection Using Cup to Disc Ratio". In this paper, the authors propose a method to calculate the CDR automatically from non-stereographic retinal fundus photographs. To automatically extract the disc, two methods making use of an edge detection method and variational level-set method are proposed in the paper. For the cup, color component analysis and threshold level-set method are evaluated. Ellipse fitting is applied to the obtained image for boundary. This method detects the edges with noise suppressed at the same time. Accuracy of this method is 89%. As depth of cup is not considered to detect its boundary, its detection is not efficient.

Abdullahi et al. (2014) presented a work which shows the effect of image resolution on the performance of automatic classification of diabetic retinopathy and storage memory. A hundred fundus images were used in this work. The fundus images were first pre-processed where the reference image pixel

resolution (size) was then reduced by 50%, 75%, 87.5% and 93.75%. For each resolution, four GLCM features were extracted and were subsequently fed to a feed forward back propagation ANN. The results in the work shows that there was no significant change in sensitivity off the first three resolutions which are 100%, the first two accuracy and specificity values were also constant which are 95.7% and 93.30%. However, the memory occupied by the images reduces significantly for every reduction in resolution. Also, there is a drop in the average classification performance for every reduction in resolution used.

Dipika and Gopichand (2015) developed a system which uses Microaneurysms as its basis of classification for the detection of Diabetic Retinopathy in fundus images of human eyes. In the achievement of such system, various preprocessing techniques including gray scale, histogram equalization, thresholding, and morphological operations were firstly performed on the fundus data. The fundus database was acquired from DRIVE – A publicly available online database for training, testing, and evaluation of digital health algorithms. Gray level 2D feature based vessel extraction was done on the fundus images after preprocessing, before a feed forward back propagation neural network was used for the detection of the microaneurysms, and hence, classifying eye as either diabetic or not. The results from the testing of the system showed an impressive sensitivity of 90% and accuracy of 90%.

Balasundari, et al (2016) proposed using image processing techniques for diagnosing retinal diseases. The diseases diagnosed were age related macula degeneration, glaucoma, retinoblastoma and diabetic retinopathy. Image processing techniques used includes binarization, median filter, thresholding, drusen detection, Gaussian filter and morphological operations. Their success rate was 90%. Limitation of this method is the use of image processing techniques alone and not a classifier algorithm. Classification by artificial neural network or support vector machine would have produced more accuracy.

(Chaudhari & Kulkarni, 2016) developed an intelligent system which uses a feed forward artificial neural network to detect the presence of Glaucoma in human eyes using the Cup-to-Disk Ratio calculation. The vertical cup-to-disc ratio (CDR) is one of the most important risk factors in the diagnosis of glaucoma. Their data acquisition was done from publicly available fundus databases which included the High Resolution Fundus (HRF) database and the DROIN database. The development of the system included several modules which included Image enhancement, image registration, image fusion, feature extraction, image segmentation, morphology operations, cup to disk ratio, and finally the classifier algorithm – Artificial Neural Network. Ideally, for a normal subject, the CDR value is typically around 0.2 to 0.3. Typically, subjects with CDR value greater than 0.6 or 0.7 are suspected of having glaucoma and further testing is often needed to make the diagnosis. The result obtained from the developed algorithm produced an accuracy of 95.74%.

Prakash and Selvathi (2017) proposed an efficient diagnostic system for screening Glaucoma disorder in the human eye using retinal images. The Optic Disc (OD) and Optic Cup (OC) were segmented from retinal images and further Neuro retinal rim region were detected. Features such as Effective Local Binary Pattern (ELBP), Gray Level Coocuurence Matrix (GLCM) and Optic Band features were then extracted from this neuro retinal rim region. These features were trained and classified using Support Vector Machine (SVM) classifier. Using this methodology, they were able to achieve 70.25% sensitivity, 99.71% specificity and 99.30% accuracy. However, only 15 images were used in this work for both training and testing.

But in this work, using standard image preprocessing techniques which will include Grayscale, Histogram Equalization and Thresholding, together with a statistical feature extraction technique, i.e., GLCM, with the aid of a Back Propagation Neural Network; two disease conditions of the Human Eye, i.e., Diabetic Retinopathy and Glaucoma, will be diagnosed by automatically analyzing the fundus images of such eye.

CHAPTER THREE

METHODOLOGY

3.1 Overview of the Eye Disease Diagnostic System

The Fig. 3.1 shows a block diagram which describes the Eye Disease Diagnostic System. This consists of data acquisition, image pre-processing, feature extraction techniques, neural network training and classification/recognition process. Two eye diseases were considered for diagnosis in this project, namely Glaucoma and Diabetic retinopathy. Details of these two diseases were presented in section 2.2

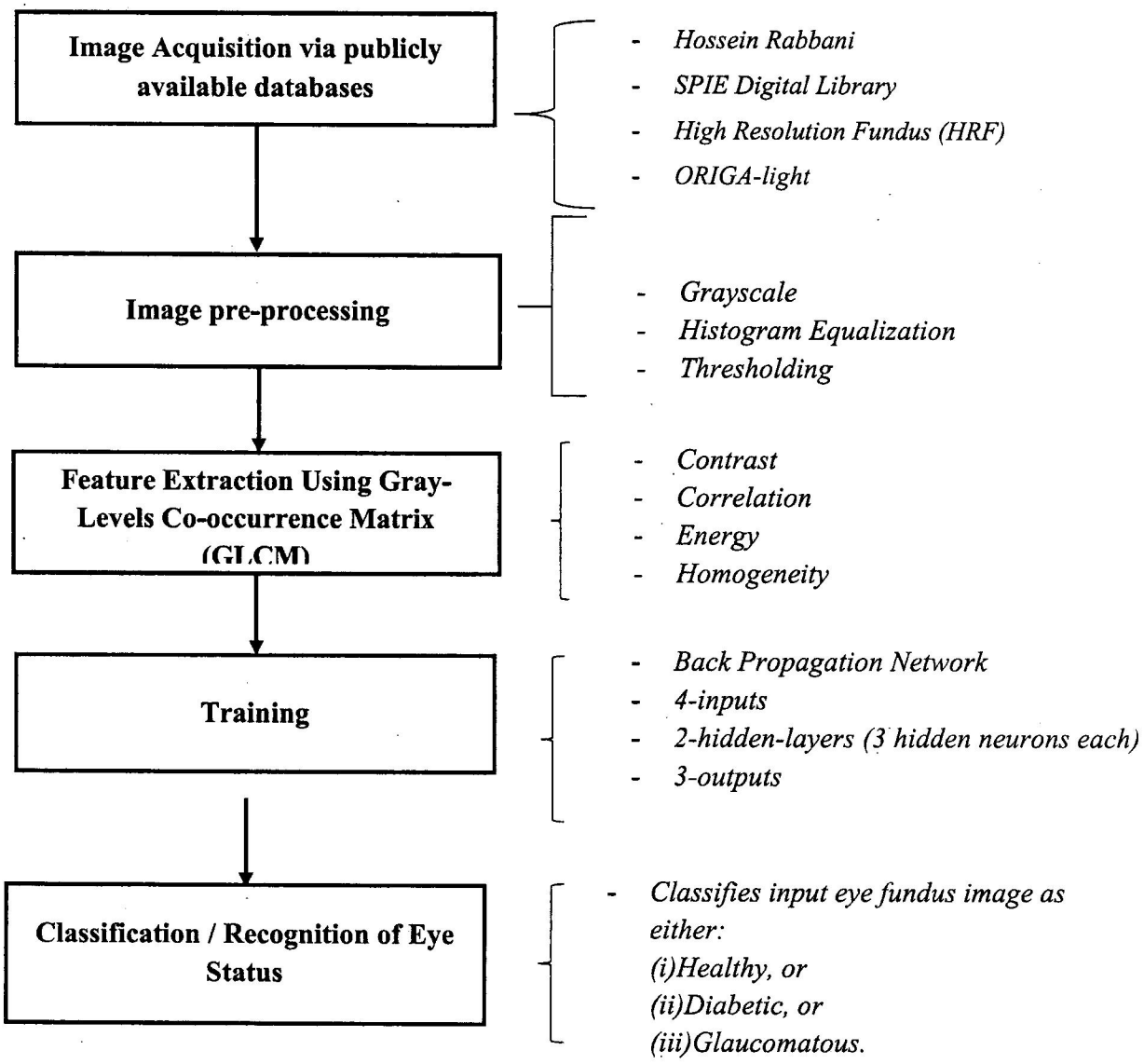

Figure 3.1: Overview of the Eye disease diagnostic system

3.2 Data Acquisition

Image acquisition is the very first step in the diagnostic system. The data acquired are the fundus images of normal(healthy) eyes and infected eyes for glaucoma and diabetic retinopathy. Publicly available datasets for all these fundus images were considered for the data required for this project. Four (4) publicly available databases were considered in the project. Details of these databases are described below:

3.2.1 Hossein Rabbani Eye Fundus Database

The fundus images in this database (Hajeb et al., 2012) was provided by the Department of Bio-electrics & Biomedical Engineering, School of Advanced Technologies in Medicine, Isfahan University of Medical Sciences, Iran. The database consists of 35 Diabetic fundus images, collected from 35 patients. The images were captured in digital form using a Canon CR5 non-mydriatic 3CCD camera at 45-degrees field of view. The images are of size 720 by 576 pixels, 8 bits per color channel and have a field of view (FOV) of approximately 540 pixels in diameter. A sample of the images acquired are shown in figure 3.2.

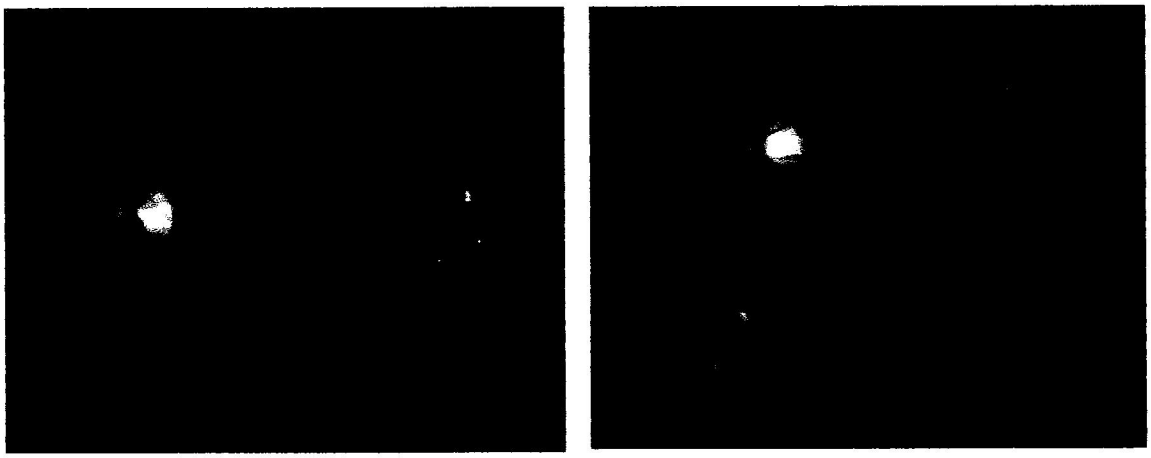

Fig 3.2: Diabetic fundus images sample acquired from Hossein Rabbani eye fundus database (Hajeb et al., 2012)

3.2.2 SPIE Eye Fundus Database

The fundus images in this dataset was provided by **SPIE** (Mahmudi et al., 2014) – A digital Library for Biomedical Applications in Molecular, Structural, and Functional Imaging, San Diego, California. The dataset contains OCT data (in mat format) and color fundus data (in jpg format) of left & right eyes of 50 healthy persons. Details of the type of fundus camera used are not provided. however, the resolution of the images are in 720 by 576. A sample of the images acquired are shown in figure 3.3.

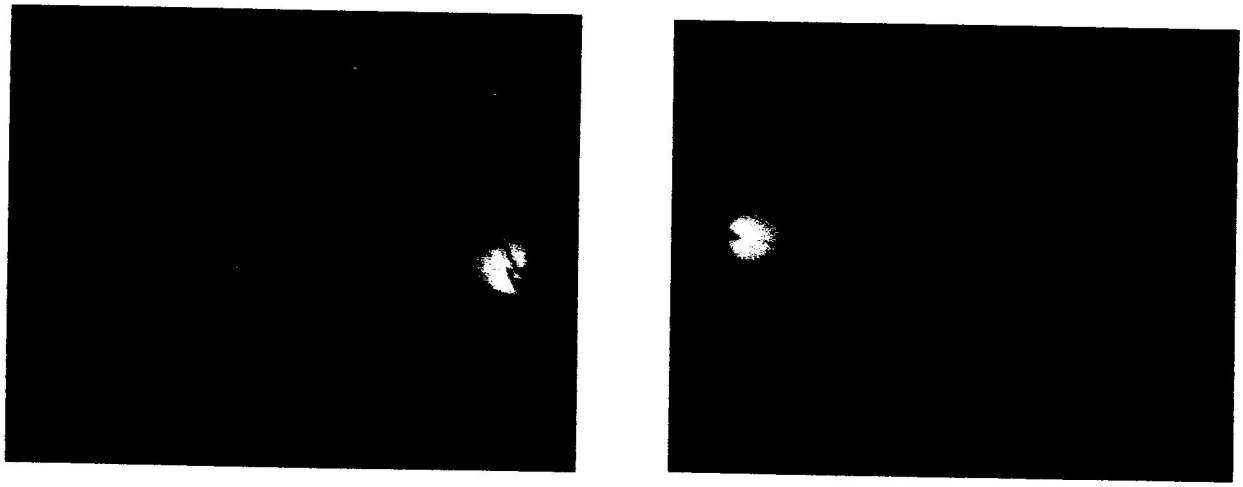

Fig 3.3: Healthy fundus images sample acquired from the SPIE database (Mahmudi et al., 2014)

3.2.3 Jan Odstrcilik Eye Fundus Database

This public database (Budai et al., 2013), provided by the Pattern Recognition Lab (CS5), the Department of Ophthalmology, Friedrich-Alexander University Erlangen-Nuremberg; contains at the moment 15 images of healthy patients, 15 images of patients with diabetic retinopathy and 30 images of glaucomatous patients. The images were captured using a Canon CR-1 fundus camera with a field of view of 45° and different acquisition setting. All images share approximately the same field of view, whereas small shifts were caused by eye movements between the acquisitions. The dataset was captured by Jan Odstrcilik. A sample of the images acquired are shown in figure 3.4.

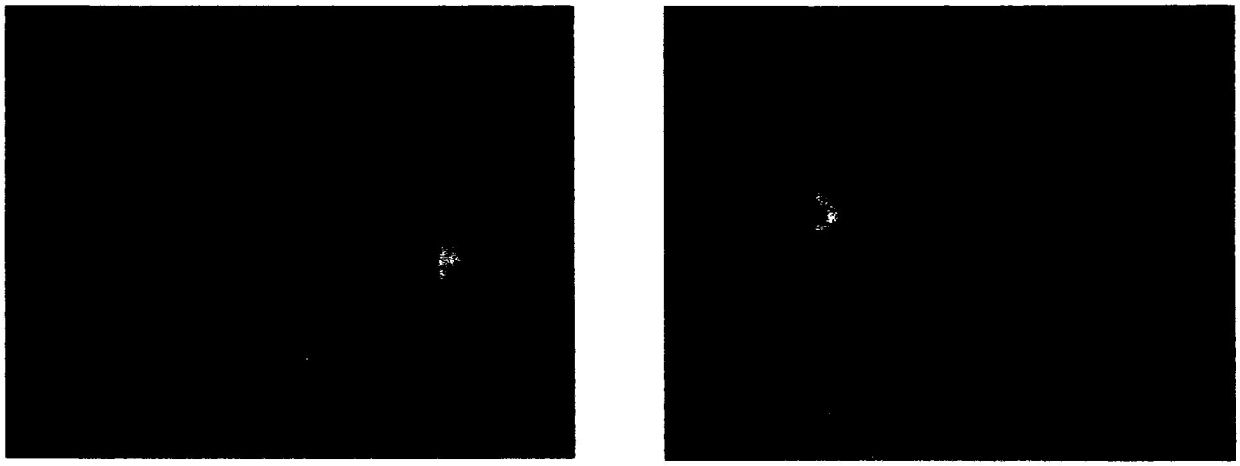

Fig 3.4: Diabetic and Glaucomatous fundus images sample acquired from the Jan Odstrcilik database (Budai et al., 2013).

3.2.4 ORIGA-light Eye Fundus Database

An online depository, ORIGA-light (Zhang., 2010), which aims to share clinical ground truth retinal images with the public; provide open access for researchers to benchmark their computer-aided segmentation algorithms. Currently, ORIGA-light contains 650 retinal images annotated by trained professionals from Singapore Eye Research Institute, which was acquired using a Canon CR-DGi fundus camera. A wide collection of image signs, critical for glaucoma diagnosis, are annotated. ORIGA-light was only available for online access upon request. The data set consists of 168 images from all glaucomatous eyes and 482 images from randomly selected normal eyes. The data set was obtained from a population based study and is therefore suitable for evaluating the performance of glaucoma screening. A sample of the images acquired are shown in figure 3.5.

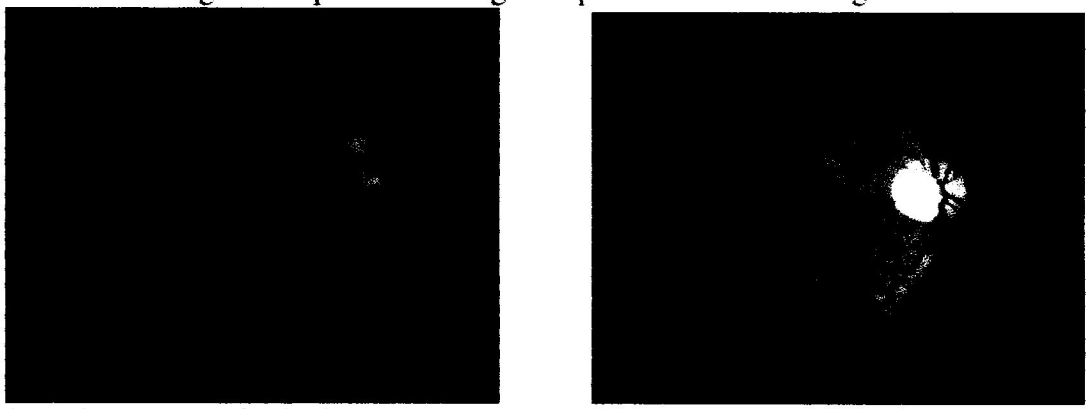

Fig 3.5: Glaucomatous fundus images sample acquired from the ORIGA-Light database (Zhang, 2010)

For the purpose of this project, the fundus image database used for training and testing the performance of the system consists total number of 135 eye images with 3 different eye conditions, where each condition has 45 fundus images each: Healthy, Diabetic Retinopathy and Glaucoma. Healthy fundus images are identified using the suffix digit "1"; Diabetic fundus images are identified using the suffix digit "2"; while Glaucomatous fundus images are identified using the suffix digit "3".

3.3 Image Preprocessing

Because of the differences in luminosity, contrast and brightness in fundus images, it makes it complex to extort retinal features and make a distinction of region of interests from other features in images (Karegowda *et al.,* 2011). Therefore, after an original fundus image is supplied into the diagnostic system, the first action required is to pre-process such image. Pre-processing is done in order to improve contrast, reduce noise, eliminate irregular illumination and bring out more details from the input image. The image preprocessing techniques for the diagnostic system includes in a sequential order, gray scale, histogram equalization and thresholding.

3.3.1 Conversion to Grayscale

Gray scale conversion is one of the simplest enhancement techniques used in image preprocessing. A grayscale digital image is an image in which the value of each pixel is a single sample, that is, it carries only intensity information. In many of the computer vision applications, color-to-grayscale conversion algorithms are required to preserve the salient features of the color images, such as brightness, contrast and structure of the color image. The colored fundus images are converted into grayscale which is two dimensional, so as to make the image suitable for processing. Figure 3.6 shows a description of a fundus image before and after grayscale.

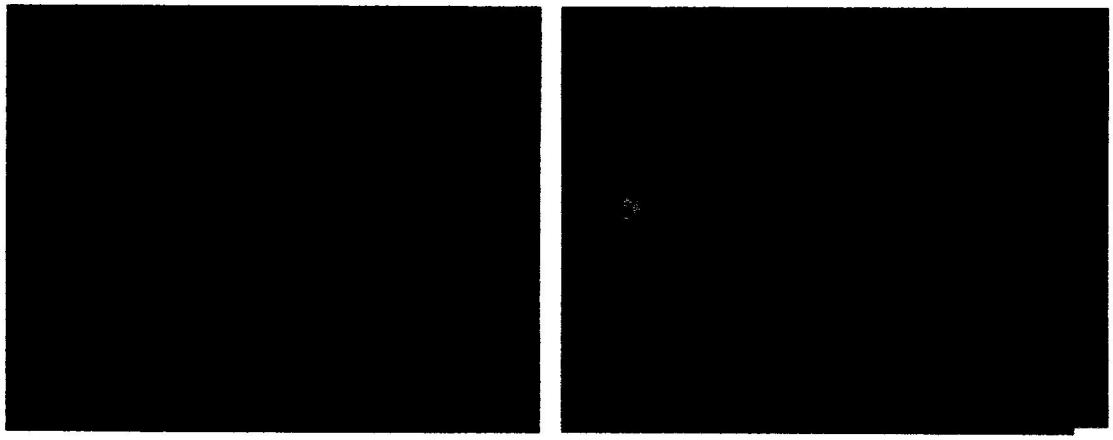

(a) Fundus image before grayscaling (b) Fundus image after grayscaling

Fig 3.6: Fundus image before and after gray scale preprocessing

3.3.2 Histogram Equalization

The fundus image usually has uneven illumination with areas at the center of the image brighter, compared to sides; and the brightness decreases as the distance from the center of the image increases (Karegowda *et al.*, 2011). To achieve uniform illumination, histogram equalization is used so that the dark area in the input image becomes brighter in the output image. The bright area that is highly illuminated remains or reduces so that the image has uniform illumination. Figure 3.7 shows a description of one of the fundus image from the project database before and after histogram equalization.

(a)Original fundus image (b) Fundus image after grayscale (c) Image after histogram equalization

Fig 3.7: Fundus images before and after histogram equalization.

3.3.3 Thresholding

In various vision applications, it is helpful to be able to separate out the regions of the image corresponding to objects in which we are interested, from the regions of the image that correspond to background. Thresholding often gives an easy and convenient method to achieve this binarization on the basis of the dissimilar intensities or colors in the foreground and background regions of an image. For the binarization of equalized image a thresholding technique is used as shown below:

Binarized Image bi, j = 255 if e (i, j) > T Else bi, j = 0. Where e (i, j) is the equalized MRI image and T is threshold resultant for the equalized image.

Figure 3.8 shows a description of a fundus image before and after all preprocessing techniques.

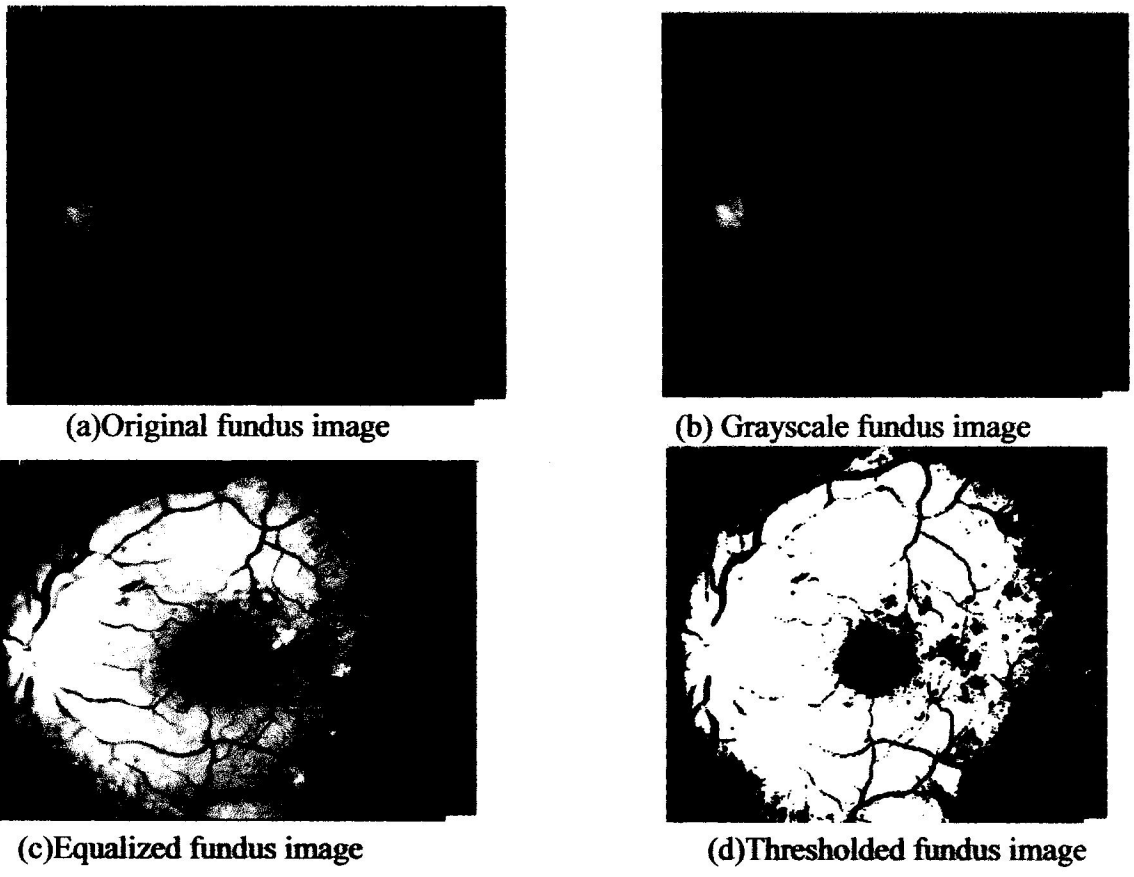

(a)Original fundus image (b) Grayscale fundus image

(c)Equalized fundus image (d)Thresholded fundus image

Fig 3.8: Graphical description of all preprocessing techniques used.

3.4 Feature Extraction using GLCM

Feature extraction is a method of capturing visual content or information from images. It is also the computation of characteristics of digital images in terms of their numerical value (Abdullahi *et al.*, 2014). Feature extraction involves the identification of the most relevant and useful characteristics and properties from a fundus image that would be the most useful in the diagnostic process of selected eye diseases. In this work, four (4) textural features based on the gray level co-occurrence matrix (GLCM) are extracted from each image. Co-occurrence matrices are calculated for four directions: 0°, 45°, 90° and 135° degrees. The four features to be extracted using GLCM includes contrast, correlation, energy and homogeneity.

3.4.1 Contrast

Returns a measure of the intensity contrast between a pixel and its neighbor over the whole image. Contrast is 0 for a constant image.

$$contrast = \sum_{n=0}^{G-1} n^2 \left\{ \sum_{i=0}^{G-1} \sum_{j=0}^{G-1} P(i,j) \right\}, |i-j| \tag{3.1}$$

3.4.2 Correlation

Returns a measure of how correlated a pixel is to its neighbor over the whole image. Correlation is 1 or -1 for a perfectly positively or negatively correlated image.

$$Correlation = \sum_{i,j} \frac{(i-\mu i)(j-\mu j)p(i,j)}{\sigma_i \sigma_j} \tag{3.2}$$

3.4.3 Energy

Energy is the property which returns the sum of squared elements for an input image, in the GLCM. For a constant image, the energy value is ideally "1".

$$Energy = \sum_{i,j} p(i,j)^2 \tag{3.3}$$

3.4.4 Homogeneity

Homogeneity is the property which returns a value that measures the closeness of the distribution of elements in the GLCM to the GLCM diagonal. Homogeneity is 1 for a diagonal GLCM.

$$Homogeneity = \sum_{i,j} \frac{p(i,j)}{1+|i-j|} \quad (3.4)$$

3.5 Diagnosis/Classification with Artificial Neural Networks

Classification in pattern recognition is a procedure for sorting pixels and assigning them to specific group or categories using classifiers. Pixels are characterized by features such as texture, gray value, color and so on (Abdullahi *et al.*, 2014). Artificial neural networks (ANN) is a computational tool, made up of highly interconnected artificial neurons that mimic the behavior of the brain (Abdullahi *et al.*, 2014). They are used for modelling complex real-world problems and to perform computations like pattern recognition, pattern matching, classification and forecasting. ANN learns by changing its synaptic weight (Sheeba & Sukeshkumar, 2009).

For the classification purpose of this project, the four features extracted from the input fundus images (using GLCM during feature extraction stage) were fed into a Back Propagation Neural Network (BPNN) classifier. This Back Propagation Neural Network (BPNN) classifier was used for classification of the fundus image into normal (healthy) or abnormal (glaucoma and diabetic retinopathy) in a supervised learning system.

3.5.1 Training and Detection of eye disease using Back Propagation Neural Network (BPNN)

The training of a back propagation network involves the three stages. The feed forward of the input training pattern, the calculation and the back propagation of the associated error and the weighted adjustment. After the network has been trained, its application involves only the feed forward phase. A multi-layer network can learn only input patterns to an arbitrary accuracy. A weight in a neural network is a segment of the information about the input signal that has to be stored.

Back propagation training takes place in 3 stages.

I. Feed forward of the input training pattern.

II. Back propagation of the associated error

III. Weight adjustment.

During feed forward, each input neuron receives an input signal and broadcasts it to the each hidden neuron, which in turn computes the activation and passes it on to its output unit, which again computes the activation to obtain the net output.

3.5.2 Hidden Layer and Neuron

In a neural network, a hidden layer neuron is a neuron whose output is connected to the inputs of other neurons and is therefore not visible as a network output (hence the term hidden layer). The hidden layer (and neurons) form the whole "interconnected neurons" concept on which neural networks are based on. a hidden layer neuron is a pre-synaptic neuron because it is connected to other neurons in the network which are post-synaptic in relation to its output.

3.5.3 Threshold Function

A threshold function is one of a series of activation functions that are used when performing classification in neural networks. In the case of the threshold function, any values above or equal to a given threshold are converted to 1, while anything falling below it is converted to a 0 during activation.

During training, the net output is compared with the target value, while the threshold function is used to determine the activation response of the network, and then from this, the appropriate error is calculated. From the error, the error factor (delta K) is obtained which is used to distribute the error back to the hidden layer. The weights are updated accordingly. In a similar manner, the error factor b (delta j) is calculated for units Zi. After the error factors are obtained, the weights are updated simultaneously. Figure 3.10 shows the procedure for the training and testing phase of the phase.

After computation of the reduced vectors of dataset, back propagation algorithm is used to train the neural network. The learning process of the BPNN is described step-by-step as follows.

Step 1: Initialize the weights and set the learning rate and the stopping criteria.

Initialize the weights w_{ij}^{l} to small random values between -1 and +1. Set the learning rate and stopping criteria.

Step 2: Randomly choose an input and the corresponding target.

Randomly choose (with replacement) an input vector $\{I_1^I,\ I_2^I, I_3^I, \ldots, I_{N^1}^I\}$ from I and the corresponding target $\{t_1, t_2, t_3, \ldots, t_{N^{L+1}}\}$ from T.

Step 3: Compute the input to each layer, and the output of the final layer.

Compute the input to each layer, $\{I_1^l,\ I_2^l, I_3^l, \ldots, I_{N^l}^l\}$, and output $\{O_1, O_2, O_3, \ldots, O_{N^{L+1}}\}$ coming out of layer L.

$$I_j^2 = \sum_{i=0}^{N^t} I_i^1\, w_{ij}^l \qquad for\ i = 1, 2, 3, \ldots, N^2 \tag{3.5}$$

$$I_j^l = \sum_{i=0}^{N^{l-1}} \mathrm{A}\,(I_i^{l-1})\ w_{ij}^{l-1} \qquad \begin{matrix} for\ i = 3, 4, 5, \ldots, L, \\ for\ j = 1, 2, 3, \ldots, N^l \end{matrix} \tag{3.6}$$

$$O_j = \sum_{i=0}^{N^L} \mathrm{A}\,(I_i^L)\ w_{ij}^L \qquad for\ j = 1, 2, 3, \ldots, N^{L+1} \tag{3.7}$$

Step 4: Compute the sensitivity components.

Compute the sensitivity components $\{\delta_1^l, \delta_2^l, \delta_3^l, \ldots, \delta_i^l, \ldots, \delta_{N^l}^l\}$

$$\delta_i^{L+1} = 2(O_i - t_i) \qquad for\ i = 1, 2, 3, \ldots, N^{L+1}. \tag{3.8}$$

$$\delta_i^l = \mathrm{A}'(I_i^l) \sum_{j+1}^{N^{l+1}} w_{ij}^l \delta_j^{l+1} \qquad \begin{matrix} for\ l = L, L-1, L-2, \ldots, 2; \\ for\ i = 1, 2, 3, \ldots, N^l \end{matrix} \tag{3.9}$$

Step 5: Compute the gradient components and update the weights.

$$\left.\begin{aligned} g_{ij}^{l} &= \frac{\partial e}{\partial w_{ij}^{l}} = \mathrm{A}\left(I_i^l\right)\delta_j^{l+1} \\ w_{ij}^{l} &= w_{ij}^{l} - r g_{ij}^{l} \end{aligned}\right\} \quad \begin{aligned} &for\ l = 1,2,3,\ldots,L \\ &for\ i = 1,2,3,\ldots,N^{l} \\ &for\ j = 1,2,3,\ldots,N^{l+1} \end{aligned} \tag{3.10}$$

Step 6: Check against the stopping criteria. Exit and return the weights or loop back to Step 2.

(a) Increment iteration index, $k = k + 1. If\ \ k > k_{Max}$, EXIT and return weights. Else,

(b) Check for convergence if $\left|g_{ij}^{l}\right| \leq g_{Min}\ for\ every\ l = \{1,2,3,\ldots,L\}$,

$$i = \{0,1,2,\ldots,N^{l}\}, and\ j = 1,2,3,\ldots,N^{l+1} \tag{3.11}$$

EXIT and return the weights. Else, loop back to step 2. Figure 3.5a shows a graphical description of one of the training phases of the network.

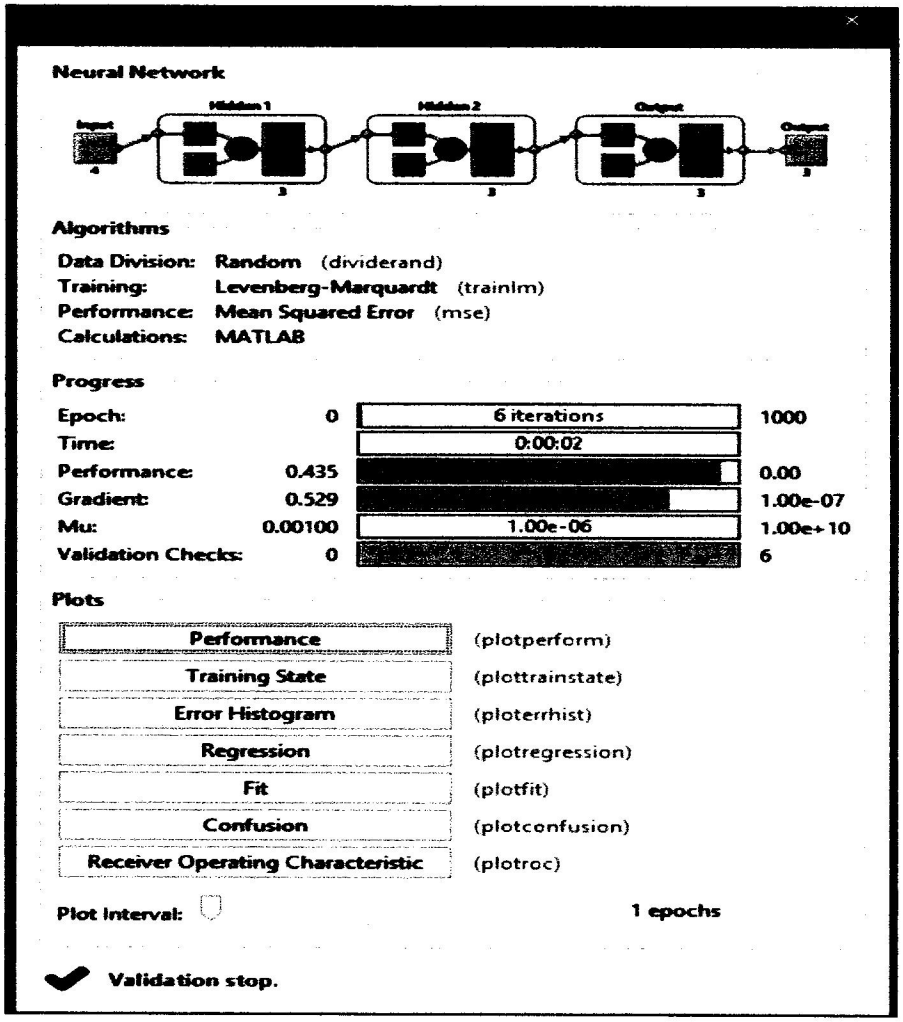

Fig 3.9: Description of the Neural network during training phase

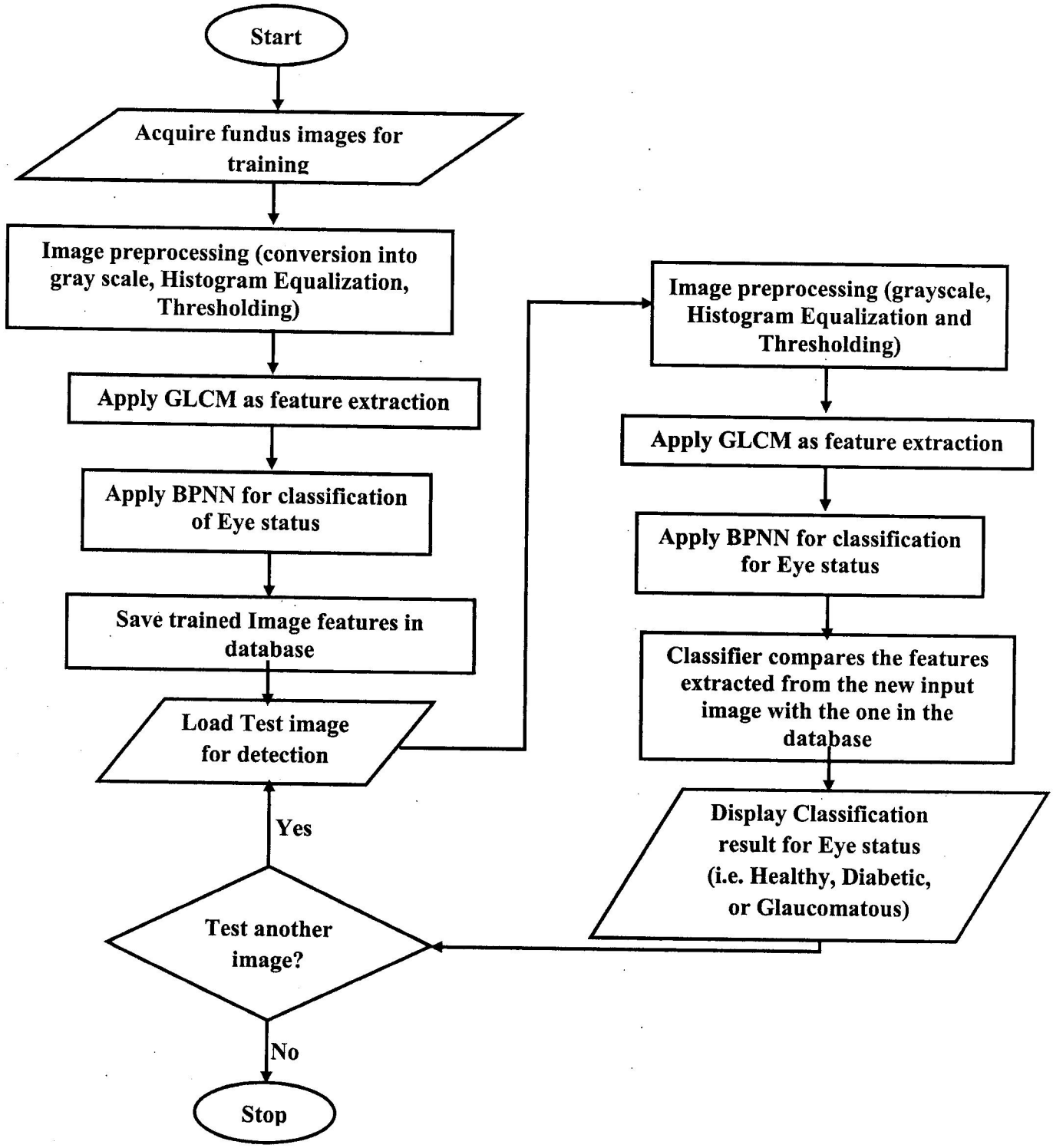

Figure 3.10: Flowchart showing training and testing phase for the diagnostic system with BPNN.

3.6 Experimental Setup

This project was developed using MATLAB software as a standalone application. The Setup is divided into four (4) major categories which are: Data Acquisition, Data Preprocessing, Feature Extraction, and Neural Network Classification. The fundus database used during the implementation of this project consists of a total of 135 fundus images. All the 135 fundus images were used in the training of the developed system, while 60 were then separated in order to do proper testing and evaluation. These fundus images were acquired from four (4) publicly available fundus databases online; the databases are: Hossein Rabbani Eye Fundus Database, SPIE Eye Fundus Database, Jan Odstrcilik Eye Fundus Database, and ORIGA-light Eye Fundus Database.

Both the training and the testing fundus images were passed through the preprocessing stage in order to remove unwanted noise, solve the problem of uneven illumination, prevent their salient features, remove any form of background interference and preserve the most needed region of interest in the image for the sake of feature extraction. The preprocessing stage included grayscale conversion, histogram equalization, and thresholding. Feature extraction was done using Gray Levels Co-occurrence Matrix (GLCM) and four textural features were extracted from each fundus image in form of positive integers. The four features are: Contrast, Correlation, Energy and Homogeneity. These four features served as the input into the Back Propagation Neural Network Classifier Algorithm.

The Back Propagation Neural Network is mostly popular for its ability to minimize errors in classification. It does this by feeding back the errors encountered after a feed-forward of inputs and then applies these errors to the inputs and updates its weights. The Hidden Layer configuration used in the classifier algorithm for the training were two hidden layers and three hidden neurons each (fed into each layer) at a threshold value '0.6'.

3.7 Performance Evaluation of the Eye Disease Diagnostic System

The performance of the Back Propagation Neural Network (BPNN) on trained and detected eye disease was evaluated based on detection accuracy, sensitivity (i.e. True positive rate) and specificity (i.e. True negative rate). Confusion matrix was used to measure the accuracy. It contains **TP, FP, FN and TN**. The details of the result of this evaluation is presented in the chapter four.

TP (True Positive) contains number of images that are correctly identified as positive. **FP** (False Positive) contains the number of images which are negative but predicted as positive. **TN** (true negative) is number of images that are negative and predicted as negative. **FN** (false negative) is number of images that are positive but predicted as negative. Sensitivity, specificity and accuracy are calculated by using these terms.

$$\text{Recall or Sensitivity}(\textit{True Positive Rate}) = \frac{\text{TP}}{\text{TP} + \text{FN}} \tag{3.12}$$

$$\text{Specificity } (\textit{True Negative Rate}) = \frac{\text{TN}}{\text{TN} + \text{FP}} \tag{3.13}$$

$$\text{Overall Accuracy} = \frac{\text{TP} + \text{TN}}{\text{TP} + \text{TN} + \text{FP} + \text{FN}} \tag{3.14}$$

CHAPTER FOUR

IMPLEMENTATION AND RESULTS

4.1 Implementation

In fulfilment of the second objective, this project was implemented in form of a software system. A graphical user interface (GUI) was designed for the system, which was developed using MATLAB, and later integrated to act as a standalone application software. It has several push buttons for loading image, pre-processing, feature extraction and ANN classification. It has a pushbutton for training of the neural network and another pushbutton for the testing of any/all class of test images. It has two axes for image display, two tables, the first table displays the textural features extracted from the input image, while the second table displays the output response of the system to input images. It also has a panel for ANN training parameters i.e. hidden layers and neurons. Finally, it also has a Reset button which when pressed clears the input data. Figure 3.11 shows the GUI for the software execution of the project.

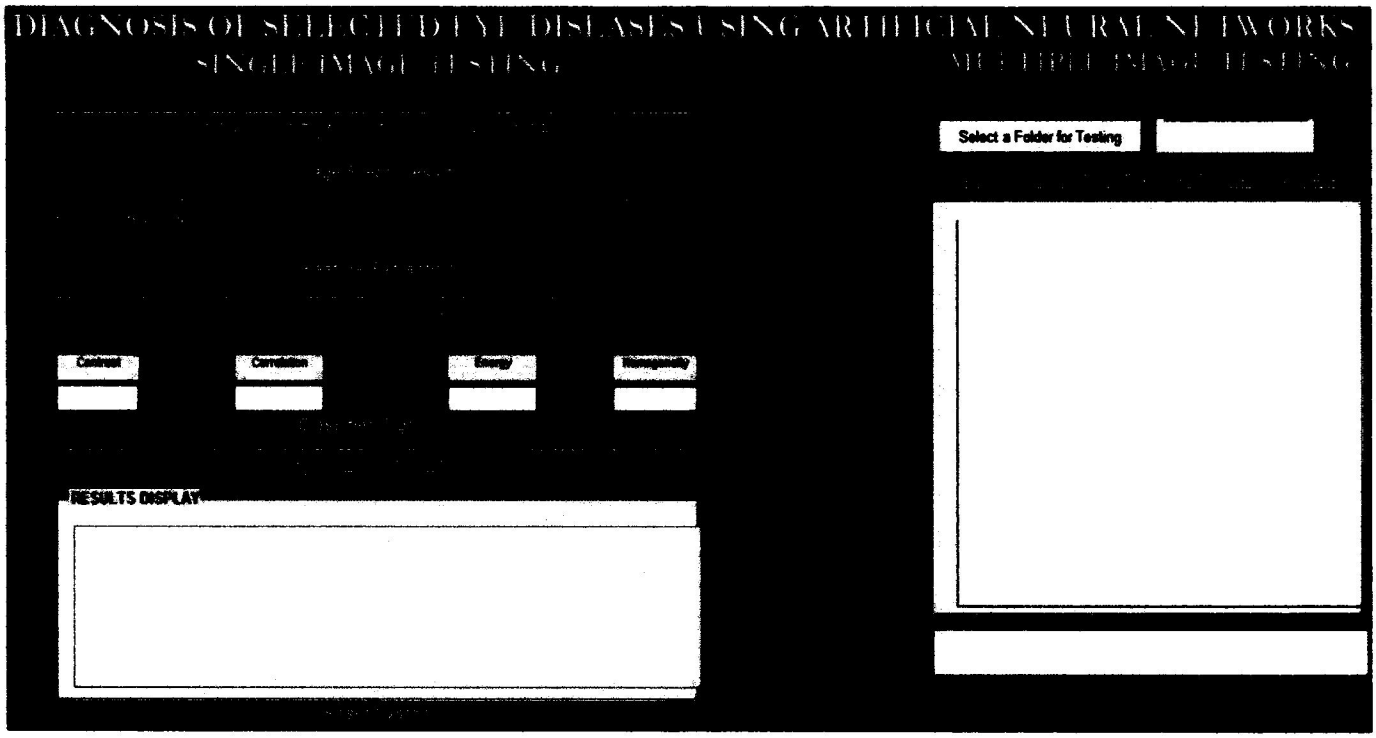

Fig 4.1: GUI display for software implementation with features extracted and image diagnosed.

4.2 Determination of Neural Network Parameters

An empirical evaluation was done on the back propagation neural network (BPNN) classifier, based on the parameters to be used for training including Threshold and hidden layer configuration, in order to determine the optimal Neural Network.

4.2.1 Determination of Hidden Layer Configuration

The NN was first repeatedly trained using four different hidden layers and neurons parameters, at a constant threshold of 0.9 (the default threshold of NNs). Table 4.1 shows the performance of the NN using three hidden layers, fed with three hidden neurons each (3-3-3); two hidden layers, fed with three hidden neurons each (3-3); three hidden layers, fed with five hidden neurons each (5-5-5); and finally for two hidden layers, fed with five hidden neurons each (5-5), all at a threshold of 0.9. The results clearly show that the classifier when trained using two hidden layers, fed with three hidden neurons each (3-3) performed better with an accuracy of 87.8%, compared to 50.4%, 51.1% and 50.4% for (3-3-3), (5-5-5) and (5-5) respectively as shown in table 4.1.

Table 4.1: System performance results for different NN parameters

No of hidden layers & neurons	Threshold value	Classifier accuracy (%)
3-3-3	0.9	50.4
3-3	0.9	87.8
5-5-5	0.9	51.1
5-5	0.9	50.4

To further illustrate the results, confusion matrices were plotted using the output and target of the classifier for each parameter. Figure 4.1 shows the confusion matrices of the NN plotted using (3-3-3), (3-3), (5-5-5), and (5-5) as hidden layers and neurons parameter, all at 0.9 threshold. The confusion

matrices show the number of images in each class (healthy (1) or DR (2) or Glaucoma (3)), they show the number of images and percentages that are correctly classified and those that are wrongly classified. Figure 4.1a is the confusion matrix for the NN trained with (3-3-3) hidden layer & neuron parameter at 0.9 threshold. 29 images were correctly classified as healthy, 5 correctly classified as DR, 34 correctly classified as Glaucoma, 27 healthy images wrongly classified as DR, 4 DR images wrongly classified as healthy, 6 healthy images wrongly classified as Glaucoma, 12 Glaucoma images wrongly classified as healthy, 5 DR images wrongly classified as Glaucoma , and 13 Glaucoma images wrongly classified as DR. Overall, 68 images were correctly classified and 67 wrongly classified which gives the accuracy of 50.4%.

Figure 4.1b is the confusion matrix for the NN trained with (3-3) hidden layer & neuron parameter at 0.9 threshold. 39 images were correctly classified as healthy, 40 correctly classified as DR, 39 correctly classified as Glaucoma, 6 healthy images wrongly classified as DR, 3 DR images wrongly classified as healthy, 0 healthy image wrongly classified as Glaucoma, 2 Glaucoma images wrongly classified as healthy, 6 DR images wrongly classified as Glaucoma, and 1 Glaucoma image wrongly classified as DR. Overall, 118 images were correctly classified and 17 wrongly classified which gives the accuracy of 87.8%.

Figure 4.1c is the confusion matrix for the NN trained with (5-5-5) hidden layer & neuron parameter at 0.9 threshold. 29 images were correctly classified as healthy, no image correctly classified as DR, 40 correctly classified as Glaucoma , 26 healthy images wrongly classified as DR, 0 DR images wrongly classified as healthy, 5 healthy images wrongly classified as Glaucoma , 16 Glaucoma images wrongly classified as healthy, 0 DR image wrongly classified as Glaucoma, and 19 Glaucoma image wrongly classified as DR. Overall, 69 images were correctly classified and 66 wrongly classified which gives the accuracy of 51.1%.

Figure 4.1d is the confusion matrix for the NN trained with (5-5) hidden layer & neuron parameter at 0.9 threshold. 29 images were correctly classified as healthy, no image correctly classified as DR, 39 correctly classified as Glaucoma, 27 healthy images wrongly classified as DR, 1 DR image wrongly classified as healthy, 6 healthy images wrongly classified as Glaucoma, 15 Glaucoma images wrongly classified as healthy, 0 DR image wrongly classified as Glaucoma, and 18 Glaucoma image wrongly classified as DR. Overall, 68 images were correctly classified and 67 wrongly classified which gives the accuracy of 50.4%.

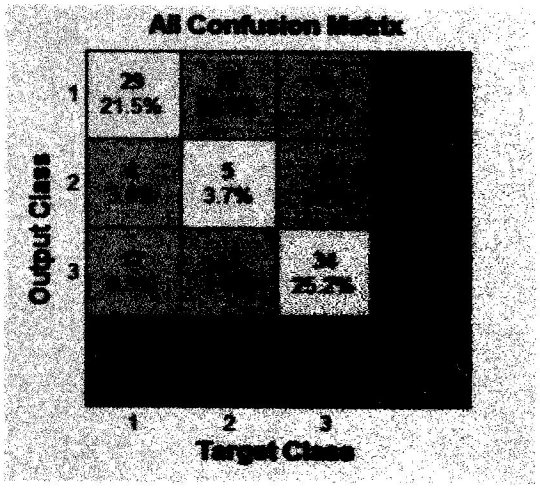

(a): HL (3-3-3)

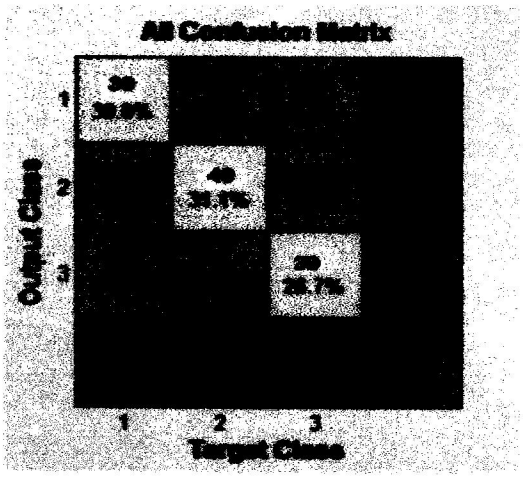

(b): HL (3-3-3)

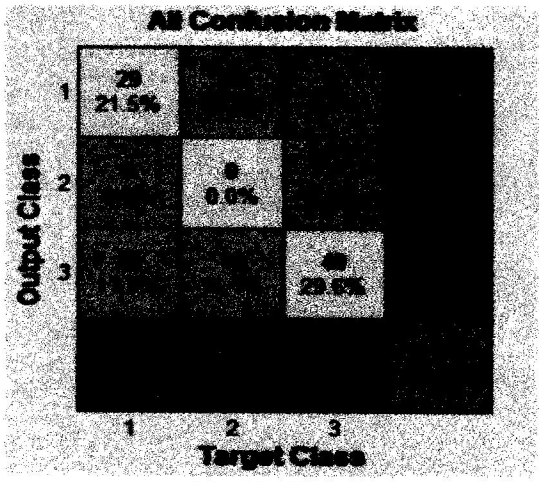

(c): HL (5-5-5)

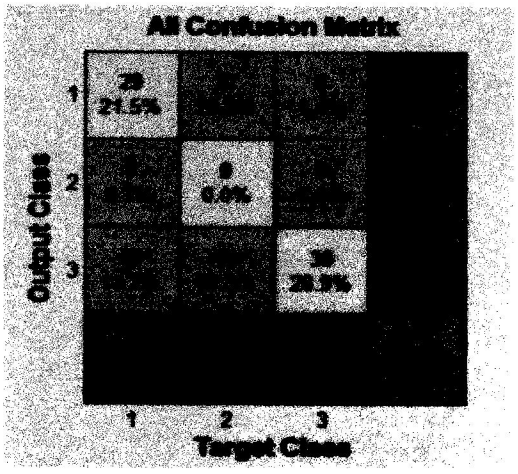

(d): HL (5-5)

Figure 4.1: Confusion matrices of NN for different hidden layer configurations at threshold 0.9

Sequel to these results, two hidden layers with three hidden neurons each (3-3) were adopted as training parameters for further determination of suitable threshold value for training and testing of the BPNN classifier.

4.2.2 Determination of Threshold value

After the best fit for hidden layers and neurons parameter had been determined, the next task was then to determine the best threshold value for which the NN will produce a response close enough to the targets. Table 4.2 shows the performance of the NN using varying threshold values of 0.9, 0.8, 0.7, 0.6, 0.5, 0.4 and 0.3, all using hidden layer and neuron parameter of "3-3". The results clearly show that the classifier when trained using two hidden layers, fed with three hidden neurons each (3-3) at a threshold value of 0.6, performed better with an accuracy of 93.3%, compared to 87.8%, 51.9%, 44.4%, 86.7%, 50% and 34% for 0.9, 0.8, 0.7, 0.5, 0.4 and 0.3 threshold values respectively as shown in the confusion matrices plotted in figure 4.2. Table 4.2 shows the number of hidden layers and corresponding neurons, threshold value and classifier accuracy. Sequel to these obtained results, two hidden layers with three hidden neurons each (3-3) and a threshold value of 0.6 were adopted as parameters for training and testing of the BPNN classifier algorithm of the developed project.

Table 4.2: System performance for different NN parameters

Hidden layer and neurons	Threshold Value	Classifier accuracy(%)
3-3	0.9	87.8
3-3	0.8	51.9
3-3	0.7	51.9
3-3	0.6	93.3
3-3	0.5	86.7
3-3	0.4	86.7
3-3	0.3	50.4

To further illustrate the results, confusion matrices were plotted using the output and target of the classifier for the threshold values considered. Figure 4.2 is the confusion matrix of the NN plotted using (3-3) hidden layers and neurons parameter, at varying threshold values of 0.9, 0.8, 0.7, 0.6, 0.5, 0.4, and 0.3. The confusion matrices show the number of images in each class (healthy (1) or DR (2) or Glaucoma (3)), they show the number of images and percentages that are correctly classified and those that are wrongly classified. Figure 4.2a is the confusion matrix for the NN trained with (3-3) hidden layer & neuron parameter at 0.9 threshold. 39 images were correctly classified as healthy, 40 correctly classified as DR, 39 correctly classified as Glaucoma, 6 healthy images wrongly classified as DR, 3 DR images wrongly classified as healthy, 0 healthy image wrongly classified as Glaucoma, 2 Glaucoma images wrongly classified as healthy, 6 DR images wrongly classified as Glaucoma, and 1 Glaucoma image wrongly classified as DR. Overall, 118 images were correctly classified and 17 wrongly classified which gives the accuracy of 87.8%.

Figure 4.2b is the confusion matrix for the NN trained with (3-3) hidden layer & neuron parameter at 0.8 and 0.7 threshold. 27 images were correctly classified as healthy, 7 images correctly classified as DR, 36 correctly classified as Glaucoma, 20 healthy images wrongly classified as DR, 8 DR images wrongly classified as healthy, 1 healthy image wrongly classified as Glaucoma, 10 Glaucoma images wrongly classified as healthy, 8 DR images wrongly classified as Glaucoma, and 18 Glaucoma image wrongly classified as DR. Overall, 70 images were correctly classified and 65 wrongly classified which gives the accuracy of 51.9%.

Figure 4.2c is the confusion matrix for the NN trained with (3-3) hidden layer & neuron parameter at 0.6 threshold. 45 images were correctly classified as healthy, 40 correctly classified as DR, 41 correctly classified as Glaucoma, 1 healthy image wrongly classified as DR, 0 DR image wrongly classified as healthy, 0 healthy image wrongly classified as Glaucoma, 0 Glaucoma image wrongly classified as healthy, 4 DR images wrongly classified as Glaucoma, and 4 Glaucoma image wrongly classified as

DR. Overall, 126 images were correctly classified and 9 wrongly classified which gives the accuracy of 93.3%.

Figure 4.2d is the confusion matrix for the NN trained with (3-3) hidden layer & neuron parameter at 0.5 and 0.4 threshold. 41 images were correctly classified as healthy, 39 correctly classified as DR, 37 correctly classified as Glaucoma, 3 healthy image wrongly classified as DR, 4 DR image wrongly classified as healthy, 0 healthy image wrongly classified as Glaucoma, 0 Glaucoma image wrongly classified as healthy, 8 DR images wrongly classified as Glaucoma, and 3 Glaucoma image wrongly classified as DR. Overall, 117 images were correctly classified and 18 wrongly classified which gives the accuracy of 86.7%.

Figure 4.2e is the confusion matrix for the NN trained with (3-3) hidden layer & neuron parameter at 0.3 threshold. 27 images were correctly classified as healthy, 6 image correctly classified as DR, 35 correctly classified as Glaucoma, 27 healthy images wrongly classified as DR, 1 DR image wrongly classified as healthy, 5 healthy images wrongly classified as Glaucoma, 17 Glaucoma images wrongly classified as healthy, 5 DR image wrongly classified as Glaucoma, and 12 Glaucoma image wrongly classified as DR. Overall, 68 images were correctly classified and 67 wrongly classified, which gives an accuracy of 50.4%.

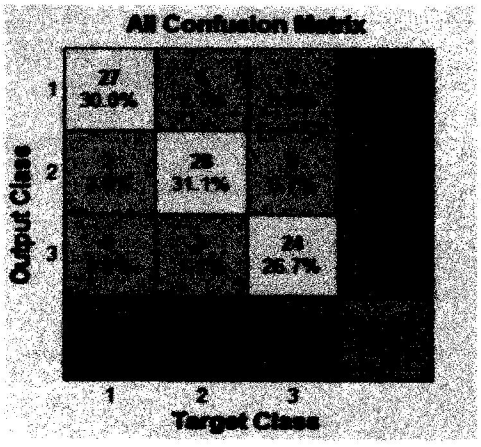

(a): HL (3-3) and threshold 0.9

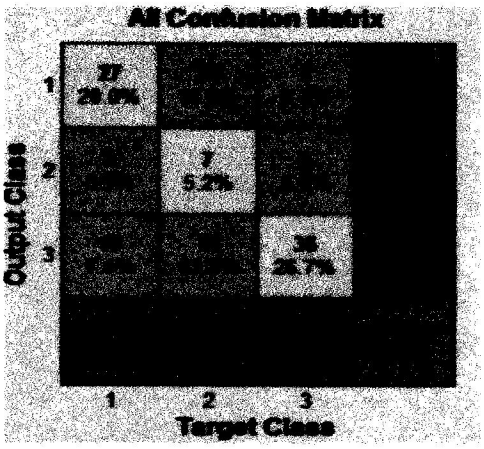

(b): HL (3-3) and threshold 0.8 and 0.7

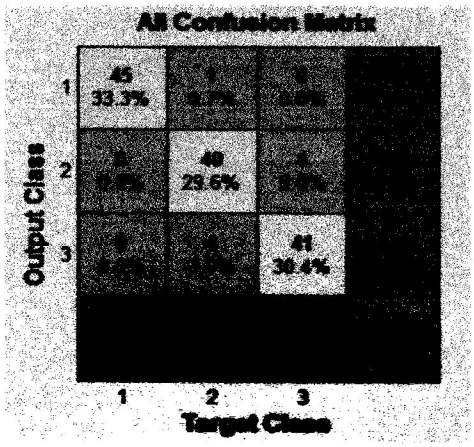

(c): HL (3-3) and threshold 0.6

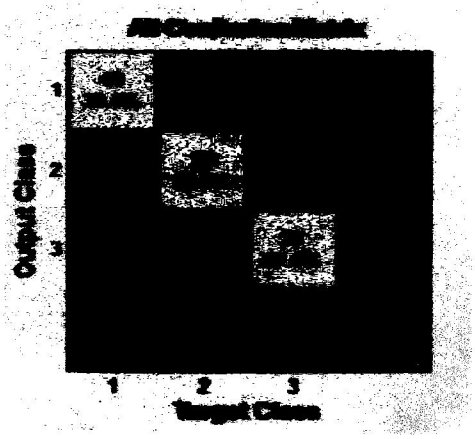

(d): HL (3-3) and threshold 0.5 and 0.4

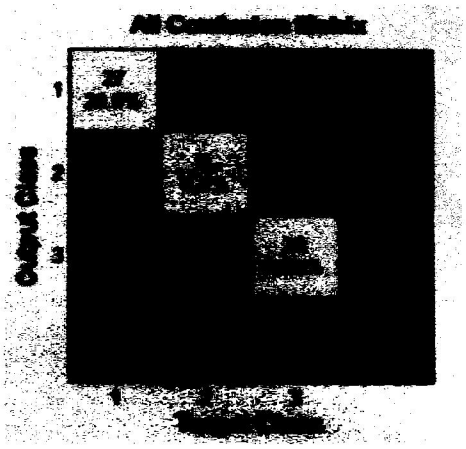

(e): HL (3-3) and threshold 0.3

Figure 4.2: Confusion matrices of NN for nine threshold values

4.3 Classification Results with Optimal Neural Network Parameters

The Classifier algorithm (BPNN) was trained to classify healthy images, diabetic retinopathy (DR) images and glaucoma images, the performance of the classifier was tested to check how many images were correctly and wrongly classified for test images. The test result for the classifier are shown in the appendix A. From the tables, all output that are tagged "1" belongs to healthy class, all output that are tagged "2" belongs to DR class, while all output that are tagged "3" is considered Glaucoma class.

Each class was tested using 20 images each from their respective test image datasets. A summary of the classification test results is shown in table 4.3.

Table 4.3: System classification test results accuracy

Eye status	Number of correct response (/20)	Accuracy (%)
Healthy	20	100
Diabetic Retinopathy	18	90
Glaucoma	19	95

In order to further illustrate the results, confusion matrices were plotted for each eye status. From Figure 4.3a, the true negative (TN), that is correctly classified healthy images are 20, and false positive (wrongly classified positive images) is 0. The percentage of the total correctly and wrongly classified images for healthy class are 100 and 0 percent respectively. From Figure 4.3b, the true positive (TP), that is correctly classified DR images are 18, and false positive (wrongly classified DR images) are 2. The percentage of the total correctly and wrongly classified images for DR class are 90 and 10 percent respectively. In figure 4.3c, the true positive (TP), that is correctly classified Glaucoma images are 19, and false positive (wrongly classified Glaucoma images) is 1. The percentage of the total correctly and wrongly classified Glaucoma images are 95 and 5 percent respectively.

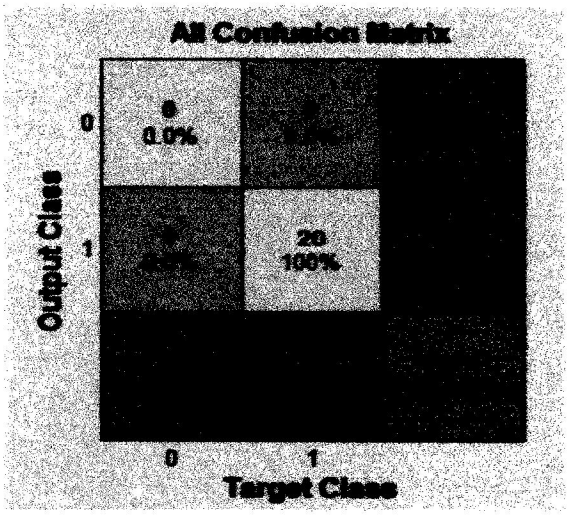

(a)Healthy images testing confusion matrix

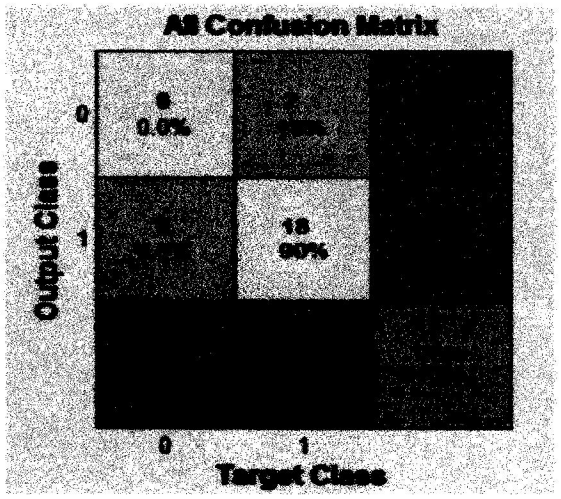

(b)DR images testing confusion matrix

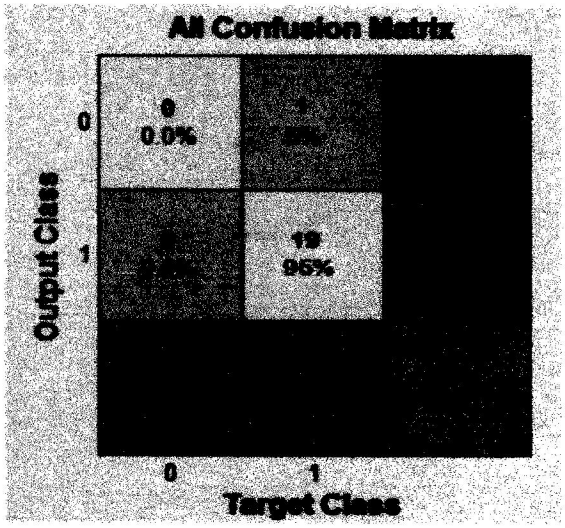

(c)Glaucoma images testing confusion matrix

Figure 4.3: Confusion matrices for classification test results

4.4 Further Discussion

The performance of the classifier for all the three classes of outputs were individually computed using the evaluation parameters explained in section 3.7. The values of TP, TN, FP, FN obtained and summarized result is presented in Table 4.4.

Table 4.4: Performance Evaluation Results

Metric	Healthy Class	DR Class	Glaucoma Class	Overall
True Positive	20	18	19	57
False Positive	0	2	1	3
True Negative	20	20	20	60
False Negative	0	2	1	3
Sensitivity	100%	90%	95%	95%
Specificity	100%	90%	95%	95%
Accuracy	100%	90%	95%	95%

The performance metrics are sensitivity, specificity and accuracy explained in section 3.6 and the results shown in Table 4.4. The sensitivity, specificity and accuracy were all calculated as 100% for the Healthy class test sample fundus images; 90% for the DR class test sample fundus images, while the Glaucoma class has 95% sensitivity, specificity and accuracy as well. The overall classification accuracy of the developed system is 95%, the overall sensitivity is 95% and overall specificity is 95%. The results obtained can therefore be summarized as follows:

The recognition of DR, Glaucoma and Healthy images was successfully achieved and the results obtained show high degree of accuracy. The summary of the results obtained for the tests carried out on the developed system is shown in Table 4.3, with the corresponding confusion matrices shown in figure 4.3. Results were obtained for a total of sixty (60) test sample fundus images (20 per class) which were used for detection and diagnosis of DR and Glaucoma, as well as recognition of normal (healthy) images. The recognition of each class was successfully done by extracting how the textural properties of fundus images vary with each other in pixel, through the help of the Gray scale co-occurrence matrix feature extraction technique, and feeding these properties into a back propagation

network for training. These features are then saved into the NN's database and used for comparing new inputs (testing).

During the testing phase, two of DR images were recognized as Glaucoma by the system, and vice-versa, due to slight resemblance of some of the fundus images of the two classes. However, both classes still managed to achieve an accuracy of 90% and 95% respectively.

Furthermore, even though this project is not a replacement for manual dilations and screening, the results show better performance compared to manual method of screening in terms of time of screening and convenience. Manual dilation of one eye takes about 15 to 20 minutes (Chalinee *et al.*, 2013) while this system takes only about 13 seconds to screen one eye.

And finally, the system was able to check for major retinal textural properties using texture features extraction algorithm to classify fundus images into three (3) classes and achieved a system accuracy of 95%; this makes this system better and less complex.

4.5 Performance Comparison with Similar Systems

In order to further validate the developed system, a performance comparison was carried out. Table 4.5 shows the performance comparison between the developed system and existing similar systems. From the table, it was observed that the developed system performance is better in terms of the specificity and accuracy compared to some of earlier developed systems in literature review.

Noronha (2006) developed an algorithm that diagnoses glaucoma using image enhancement techniques and hough transform and achieved an accuracy of 93%. Furthermore, with the aim of diagnosing for glaucoma, Bock et al (2007), L´aszl´o (2009) and Vahabi (2010) used texture based features, support vector machine & Sobel edge detection and Template matching respectively and achieved accuracies of 86%, 86% and 89.4%. Ramani (2012) developed a system which was used to diagnose diabetic retinopathy and glaucoma from fundus images using data mining techniques and achieved an accuracy

of 92%, while Chalinee et al (2013) using image processing techniques was able to develop a more comprehensive algorithm that diagnosed four eye statuses - Age Related Macula Degeneration (AMD), Glaucoma, Retinoblastoma and DR – and was able to attain a high accuracy of 90%. A summary is presented in table 4.5 below:

Table 4.5: Performance comparison between the developed system and similar existing systems

Authors	**Classifier Algorithm**	**Accuracy**	**Diseases recognized**
Kevin Noronha (2006)	Enhancement techniques and hough transform	93%	Glaucoma.
Bock et al (2007)	Texture based features	86%	Glaucoma.
L´aszl´o (2009)	Support Vector Machine	86%	Glaucoma.
Vahabi (2010)	Sobel edge detection and Template matching	89.4%	Glaucoma.
Ramani (2012)	Data mining techniques	92%	Glaucoma and DR.
Chalinee et al (2013)	Image processing techniques	89%	Glaucoma.
Balasundari, et al (2016)	Image processing techniques	90%	ARMD,Glaucoma, Retinoblastoma and DR.
Developed System	GLCM and Back Propagation Neural Network	95%	Glaucoma, Diabetic Retinopathy.

CHAPTER FIVE

CONCLUSION AND RECOMMENDATIONS

5.1 Summary

This project proposed and implemented an intelligent diagnostic system for selected human eye diseases; a system whose implementation can be used for screening of patients eyeballs (fundus image) for detecting glaucoma and diabetic retinopathy in a cost effective manner, most importantly, detecting it in its early stage and thus preventing eventual vision loss or blindness. The actualization of this project involved four major stages. The first was preprocessing of the fundus (input) images using three image pre-processing techniques – Grayscaling, Histogram equalization, and Thresholding. After preprocessing, feature extraction was performed on the preprocessed images. A textural feature extraction technique was employed in order to measure how the images vary with each other in pixel values, and this was done using the Gray Levels Co-occurrence Matrix (GLCM). Four GLCM features were extracted namely contrast, correlation, energy and homogeneity, and these served as the four inputs fed into the back propagation artificial neural network (BPNN) for training. The classifier algorithm (BPNN) was trained and tested using these extracted features on a total of 135 eye fundus images.

The performance analysis results show that the BPNN when trained using two hidden layers, fed with three hidden neurons each at a threshold value of 0.6 has a better accuracy of 93.3%. The developed system's classification result for the BPNN classifier shows that the classifier attained an accuracy of 100% for healthy images, 90% for diabetic images and 95% for glaucoma images. The overall classification accuracy of the developed system is 95%, sensitivity is 95%, while same also goes for specificity, 95%.

5.2 Conclusion

This project was developed to accept fundus retinal images and successfully detect two pathological conditions with the human eye, in form of Glaucoma and Diabetic Retinopathy, associated with such eye with the use of Back Propagation Neural Network classifier algorithm. Such a system can be of

significant benefit for mass diagnosis in rural areas, especially where patient-to-ophthalmologist ratio is as high as 4,000:1 (WHO, 2011). A major advantage of this project is that the accuracy achieved for eye diseases detection is as high as 95% which makes it better and less complex.

5.3 Recommendations

This project has demonstrated the usefulness and effectiveness of artificial neural networks as a problem solving tool even in fields outside computing, such as health sector. It has also shown great performance in terms of aiding diagnosis of glaucomatous and diabetic human eye, however, it is recommended that more work still be done on:

1. Extending this project to develop similar diagnostic tools for other retinal diseases.
2. Combining it with other telemedicine applications (hybridization), so as to enhance better and more sophisticated diagnosis of various retinal diseases for remote, inaccessible and rural areas, most especially in Nigeria.
3. Implementing this project as an embedded system in order to allow better flexibility.
4. Implementation of a self-data acquiring functionality in form of camera to capture fundus or ocular images.
5. Extraction of more features for training from fundus images which may lead to increase in the accuracy.

REFERENCES

Abdullahi I. M, Arulogun O. T, Adeyanju I. A & Nuhu B. K (2015). The Effect of Image Resolution on The Performance Of Automatic Classification Of Diabetic Retinopathy And Storage Memory. IMPACT: International Journal of Research in Engineering & Technology (IMPACT: IJRET) ISSN(E): 2321-8843; ISSN(P): 2347-4599 Vol. 3, Issue 3, 29-36.

Abdullahi I. M, Arulogun O. T, Adeyanju I. A, Olaniyi O.M. & Nuhu B. K (2015). Towards A Hybrid Statistical Feature Extraction and Hierarchical Classification Model for Diabetic Retinopathy Diagnosis. Proceedings of the Third International Conference on Engineering and Technology Research August 5 - 7, ISBN: 978-2902-58-6 Volume 3.

Alamelu J.M, Wagle S, and Kumar V.S. (2015). An Improved K-Nearest Neighbor Classifier using Interestingness Measures for Medical Image Mining. Jayakumari, C.; and Santhanam, T. (2008). An Intelligent Approach to Detect Hard and Soft Exudates Using Echo State Neural Network, Information Technology Journal 7 (2), 386395.

American Cancer Society's (ACS) publication (2017), Cancer Facts and Figures. Retrieved from www.acs.org., march 18th, 2017.

Annu N & Judith J (2013). "Automated Classification of Glaucoma Images by Wavelet Energy Features,"International Journal of Engineering and Technology (IJET).

Badawi A.M, Derbala A.S & Youssef A.M. (1999). Fuzzy logic algorithm for quantitative tissue characterization of diffuse liver diseases from ultrasound images. Int J Med Inf; 55: 135 47.

Baum, L. E. & Petrie T. (1966). "Statistical Inference for Probabilistic Functions of Finite State Markov Chains". The Annals of Mathematical Statistics. 37 (6): 1554–1563. doi:10.1214/aoms/1177699147.

Baum, L. E. & Petri T. (1966). "An inequality with applications to statistical estimation for probabilistic functions of Markov processes and to a model for ecology". Bulletin of the American Mathematical Society. 73(3): 360. doi:10.1090/S0002-9904-1967-11751-8. Zbl 0157.11101.

Balasundari, C.K, Ulagammal R, Sivapriya, J., & Sakthiya, S.V. (2016). Diagnosing RetinalDiseases Using Image Processing Techniques. International Journal of Innovative Research in Computer and Communication Engineering Vol. 4, Issue 4

Baxt W.G. (1990). Use of an artificial neural network for data analysis in clinical decision-making: the diagnosis of acute coronary occlusion. Neural Computing; 2: 480–9.

Belacel N, Vincke P, Scheiff J.M, Boulassel M.R. (2001). Acute leukemia diagnosis aid using multicriteria fuzzy assignment methodology. Computer Methods Programs Biomedicine; 64: 145–51.

Bock R, Meier J, Michelson G, Nyl L.G, and Hornegger J. (2007). "Classifying glaucoma with image-based features from fundus photographs,"Proc. 29th DAGM Conf. Pattern Recognit. , pp. 355–364.

Boudaren, E.A, (2012). Dempster Shafer fusion of multisensor signals in nonstationary Markovian context, EURASIP Journal on Advances in Signal Processing, No. 134.

Budai, A; Bock R.M, Hornegger, J; & Michelson, G. (2013) Robust Vessel Segmentation in Fundus Images. International Journal of Biomedical Imaging, vol. 2013.

Chalinee B.C, Kongprawechnon W.C, Kondo T.A & Sintuwong S.K (2013). "*Image Processing Techniques for Glaucoma Detection Using the Cup-to-Disc Ratio*" Thammasat International Journal of Science and Technology, Vol. 18, No. 1.

Chaudhari C.K. and Kulkarni M.O. (2016*) Using Artificial Neural Network to Detect Glaucoma with the Help of Cup to Disk Ratio*. Department of Physics, King's College, London, UK. Diabet Med. Jan;21(1):84-90.

Clark R.K. (2005) Anatomy and Physiology: *Understanding the Human Body; Taking Health Telematics into the 21st Century.* Oxon, Radcliffe Medical Press.

Connolly T.M, Boyle E.A & Macarthur E (2012). A systematic literature review of empirical evidence on computer games and serious games. Computers & Education, 59:661-686.

Deepak K.S, Madhulika J, Gopal D.J, Sivaswamy J, (2012). "Motion pattern based image features for glaucoma detection from retinal images,"ICVGIP.

Dipika D.A. and Gopichand E.J. (2014) *Development of a system based on Artificial Neural Network for the Diagnosis of Diabetic Retinopathy.* Computational and Mathematical Methods in Medicine, vol. 2014, Article ID 672398, 15 pages,1617-1632.

Duanggate C, Bunyarit U, Stanislav S. M, Sarah B, and Williamson T. (2011) "Parameter-free optic disc detection."Computerized Medical Imaging and Graphics 35, no. 1:51-63.

Einthoven, W. (2005). Journal of Telemedicine and Telecare, 11(1):3–9.The telecardiogram.

Eysenbach, G. (2001). What is e-health? *Journal of Medical Internet Research*, *3*(2), e20. http://doi.org/10.2196/jmir.3.2.e20

Garaci, F.G., Francesca B, Cerulli A, Melis M, Arnoldo S, Claudio C, Roberto F, Giovanni Simonetti, and Carlo Nucci. (2009). "Optic Nerve and Optic Radiation Neurodegeneration in Patients with Glaucoma: In Vivo Analysis with 3-T Diffusion-Tensor MR Imaging1."Radiology252, no. 2: 496-501.

Hajeb S.H, Rabbani H, Akhlaghi M.R, (2012) "Diabetic Retinopathy Grading by Digital Curvelet Transform", Computational and Mathematical Methods in Medicine, vol. 2012, Article ID 761901, 11 pages, 2012.1607-1614.

Halm U, Rohde N, Klapdor R, Reith H.B, Thiede A, Etzrodt G. (2000). Improved sensitivity of fuzzy logic based tumor marker profiles for diagnosis of pancreatic carcinoma versus benign pancreatic disease; 20: 4957–60.

Heath G, (2006). "The episclera, sclera and conjunctiva: An overview of relevant ocular anatomy. differential diagnosis of ocular disease,"in Continuing Education and Training, p. 7, Alcon, Module 9, Part 2.

Haghighat, M.; Zonouz, S.; Mottaleb, A.M. (2013). "Identification Using Encrypted Biometrics". Computer Analysis of Images and Patterns. Lecture Notes in Computer Science. 8048. p. 440. doi:10.1007/978-3-642-40246-3_55. ISBN 978-3-642-40245-6.

Harisha, K. R. (2015), Feature Extraction Technique for Robust and Fast Visual Tracking: A Typical Review, International Journal of Emerging Engineering Research and Technology Volume 3, Issue 1.

Heinzelmann, P.J; Lugon, N.E, Kvedar, J.C. (2000). Telemedicine in the future. Taking Health Telematics into the 21st Century. Oxon, Radcliffe Medical Press.

Henriksen J.J, (2007). 3D surface tracking and approximation using Gabor filters, South Denmark University.

Iluyemi A., Jones T. and Annie S, (2012). E-health in the commonwealth: Making national e health policies and strategies work: London commonwealth secretariat, Kariyawasam.

Javitt, Miles (1986). *Computer in Medicine: Application and Possibilities*. W.B. Saunders Company, Philadelphia.

Johnson S (2006). Stephen Johnson on Digital Photography. O'Reilly. ISBN 0-596-52370X.

Karegowda A.G, Bharathi P.T, Jayaram M.A. & Manjunath A.S. (2011) "Automatic Detection of Exudates in Diabetic Retinopathy using Traditional & Machine Learning Techniques: An Overview", International Conference on Computing, New Delhi.

Kariyawasam, N. C., Weerasekera, V. S., Dayaratne, M.K. (2010). 'EIMMR: The future of health statistics in Sri Lanka'. SriLanka Journal of Bio-medical informatics, 1(Supplement 1), S14.

Ketcham D.J, Lowe R.W & Weber J.W, (1974). Image enhancement techniques for cockpit displays. Tech. rep., Hughes Aircraft.

Klein H.M, Eisele T, Klose K.C, Stauss I, Brenner M, Ameling W. (1996). Pattern recognition system for focal liver lesions using 'crisp' and 'fuzzy' classifiers. Invest Radiol; 31: 6–10.

Koyama S, Obata Y, Shimamoto K, Ishigaki T, Ishii N, Isomoto Y. (1997). Breastultrasonography: computer-aided diagnosis using fuzzy inference. J Ultrasound Med; 16: 665–72.

Kumar, P. S, & Deepashree D (2013). Automatic exudate detection for the diagnosis of DR. International Journal of Innovative Research and Studies, pp. 658-669.

L´aszl´o G. N, (2009). "Retinal image analysis for automated glaucoma risk evaluation". Medical Imaging, Parallel Processing of Images and Optimization Techniques. Proceedings of SPIE Vol.7497.

Mahmudi T, Kafieh R, Rabbani H, (2014) "Comparison of macular OCTs in right andleft eyes of normal people", in Proc. SPIE9038, Medical Imaging 2014: Biomedical Applications in Molecular, Structural, and Functional Imaging, 90381K, San Diego, California, United States Feb. 15-20, 2014. doi: 10.1117/12.2044046

Maltry A.C, Kitzmann A.S. Cataract-EyeRounds.org. (2012). Available from: http://EyeRounds.org/cases/146-morgagnian-cataract.htm

Manoujitha, Kugamourthy & Goonetileke, Oshini (2014). e-Opthalmologist Intelligent Eye Disease Diagnosis System. *Fifth International Conference on Intelligent Systems, Modelling and Simulation,* DOI 10.1109/ISMS.2014.64.

Mantas, J. (2002). Electronic health record. Studies in Health Technology & Informatics. 65:250 7.

Mark A. M, and Edward H. S. (2006). Clinical Decision Support Systems. Methods of information in medicine, DOI: 10.1007/0-387-36278-9_20

Mark S. N and Alberto S. A. (2008). Feature Extraction and Image Processing. Academic Press, p. 88.

Mason D.G, Ross J.J, Edwards N.D. (1997). Self-learning fuzzy control of atracurium-induced neuromuscular block during surgery. Med Biol Eng in Computer; 35: 498–503.

McCulloch W.S, Pitts W. (1943). A logical calculus of the ideas imminent in nervous activity. Bull Math Biophys; 5: 115–33.

Muramatsu, C, Toshiaki N, Sawada A, Yuji H, Takeshi H, Yamamoto T, and Hiroshi F. (2011)"Automated segmentation of optic disc region on retinal fundus Photographs: Comparison of contour modeling and pixel classification methods. "Computer methods and programs in biomedicine.101,no.1:23-32.

Musen, M.A. (2000). Scalable software architectures for decision support. Methods of Information in Medicine,38:229–238.

Narasimhan K.D. (2011) "An efficient automated system for glaucoma a detection using fundus image." Journal of Theoretical and Applied Information Technology33(1):104-110.

National Institutes of Health. (2006). Electronic Health Records Overview. National Institutes of Health. Retrieved from http://www.ncrr.nih.gov/publications/informatics/ehr.pdf, march 18th, 2017

Noronha, K; Jagadish N & Bhat S, (2006). "Enhancement of retinal fundus Image to highlight the features for detection of abnormal eyes" Methods of Information in Medicine,61:125–140.

Oliveira, Anarita (2014), *Design of a Mobile Application for Eye Signs Screening* (Master's Thesis). Instituto Superior de Engenharia do Porto.

Pardo B. and Birmingham, W. (2005) Modeling Form for On-line Following of Musical Performances. AAAI-05 Proc.

Prakash & Selvathi (2017), An Efficient Detection System for Screening Glaucoma In Retinal Images. Biomed. & Pharmacol. J., Vol. 10(1), 459-465 (2017)

Pooja, Chaudhari and Girish, Kulkarni. (2016). International Journal of Advanced Research in Electronics and Communication Engineering (IJARECE) Volume5,Issue 7

Ramani R.G, (2012) "Automatic Prediction of Diabetic Retinopathy and Glaucoma through Retinal Image Analysis and Data Mining Techniques"

Rao, B & Lombardi, A. (2005). Populations Journal of Telemedicine and Telecare, 11(5):221 224. Telemedicine: current status in developed and developing countries.

Remington L.A, (2012). Clinical Anatomy and Physiology of the Visual System. Elsevier, 3 ed.

Rosenblatt F. (1958). The Perceptron: a probabilistic model for information storage and organization in the brain. Psychol Rev; 65: 386–408.

Schmid, C & Mohr, R (1997). "Local grey value invariants for image retrieval," IEEE Trans Pattern Anal Machine Intell, 19, pp. 530–534.

Schneider J, Bitterlich N, Velcovsky H.G, Morr H, Katz N (2002). E. Fuzzy-logic based tumor-marker profiles improved sensitivity in the diagnosis of lung cancer. Int J Clin Oncol; 7: 145–51.

Seker H, Odetayo M.O, Petrovic D, Naguib R.G, Bartoli C, Alasio L. (2002). Assessment of nodal involvement and survival analysis in breast cancer patients using image cytometric data: statistical, neural network and fuzzy approaches. Anticancer Res; 22: 433–8.

Selmi P.M, Klein M.H, Greist J.H et al (1990). Computer administered cognitive-behavioral therapy for depression. American Journal of Psychiatry,147:51-56.

Sekhar S, (2008). "Automated localisation of retinal optic disk using hough transform", Department of Electrical Engineering and Electronics, University of Liverpool, UK.

Shapiro S.C. (1992) Artificial intelligence. In: Shapiro SC. (ed) Encyclopedia of Artificial Intelligence, vol. 1, 2nd edn. New York: Wiley.

Sheeba O and Sukeshkumar A, (2009). "Neural Networks in the diagnosis of Diabetic Retinopathy," International conference on Modelling and Simulation (MS'09), Trivandrum, Kerala, pp. 256-259.

Singh, D., & Kaur, K. (2012), "Classification of Abnormalities in Brain MRI Images Using GLCM, PCA and SVM", International Journal of Engineering, Vol. 1, pp. 2249-8958.

Sinthanayothin, Chanjira; Viravud, Kongbunkia; Suthee, Phoojaruenchanachain, and Apichart Singlavanija. (2003) Automated screening system for diabetic retinopathy. In Proceedings of the 3rd International Symposium on Image and Signal Processing and Analysis, pages 915 920.

Sood S.P. (2006). Archives of Disease in Childhood, Differences in public and private sector adoption of telemedicine: Indian case study for sectoral Adoption. Studies in Health Technology and Informatics, 130:257–268.

Starner T, Pentland A. (1995). Real-Time American Sign Language Visual Recognition From Video Using Hidden Markov Models. Master's Thesis, MIT, Feb 1995, Program in Media Arts

Stratonovich, R.L. (1960). "Conditional Markov Processes". Theory of Probability and its Applications. 5 (2): 156–178. doi:10.1137/1105015.

Strehle E.M., Shabde N. (2006) One hundred years of telemedicine: does this new technology have a place in paediatrics? Archives of Disease in Childhood, 91(12):956–959.

Szolovits, Peter (1982). *Artificial Intelligence in Medicine*. West View Press Inc., Colorado.

Strehle E.M., Shabde N. (2006) One hundred years of telemedicine: does this new technology have a place in paediatrics? Archives of Disease in Childhood, 91(12):956–959.

Sund T & Moystad A. (2006) Sliding window adaptive histogram equalization of intra-oral radiographs: effect on diagnostic quality. Dentomaxillofac Radiol. May;35(3):133-8.

Tahseen A. J, Yasin H, & Yasin M.M, (2011), "PCA-ANN for Classification of Hepatitis-C patients". International Journal of Computer Applications, Vol. 14, Issue 7, pp. 0975-8887.

Usher D, Dumskyj M, Himaga M, Williamson T.H, Nussey S, and Boyce J. (2003). Automated detection of diabetic retinopathy in digital retinal images: a tool for diabetic retinopathy screening. Diabetes UK. Diabetic Medicine, 21:84–90.

Vahabi Z, (2010). "The new approach to Automatic detection of Optic Disc from non-dilated retinal images" Proceedings of the 17th Iranian Conference of Biomedical Engineering (ICBME2010).

Walter, T; Jean-Claude, K; Pascale M; and Ali E. (2002). A contribution of image processing to the diagnosis of diabetic retinopathy - detection of exudates in color fundus images of the human retina. IEEE Transactions on Medical Imaging, 21:1236 1243.

Wandell B.A. (2014), Foundations of Vision. The Photoreceptor Mosaic, Stanford University.

Werbos P. (1974). Beyond regression: new tools for prediction and analysis in the behavioral sciences. PhD Thesis, Harvard University .

Wootton R, Menzies J, Ferguson P. (2009). Journal of Drugs in Dermatology, (371–375). Followup data for patients managed by store and forward telemedicine in developing countries.

Wootton R. (2009). Journal of Telemedicine and Telecare, 15(2):83–88. The development of telemedicine. In: Rigby, Roberts, Thick, eds.

Wootton R. (2005). Journal of Telemedicine and Telecare, 11(8):384–390. Telemedicine support for the developing world.

World Health Organization (2006a). Report on chronic diseases in world communities. Retrievedfrom *www.who.int* on march 22nd, 2017.

World Health Organization (2006b), Report of a WHO Working Group: *Vision 2020 Global initiative for the elimination of avoidable blindness: action plan 2006- 2011.* Geneva; 2002:34–44.

World Health Organization (2014). State of the art on common diseases. Retrieved from *www.who.int* on march 22nd, 2017.

World Health Organization (2015). Chronic diseases Report. Retrieved from *www.who.int/chp/chronic_disease_report* on march 22nd, 2017.

Wright J.H, Wright A.S (1997). Computer-assisted psychotherapy. Journal of Psychotherapy Practice and Research, 6:315-329.

Yegnanarayana B, (1999) Artificial neural networks, Prentice- Hall of India private limited.

Zadeh LA. (1965) Fuzzy sets. Inf Control; 8: 338–53. 47.

Zadeh LA. Biological application of the theory of fuzzy sets and systems. (1969). Proceedings of the International Symposium on Biocybernetics of the Central Nervous System. Boston: Little Brown; 199–212.

Zhang, Zhuo (2010). "ORIGA-light : An Online Retinal Fundus Image Database for Glaucoma Analysis and Research", 32nd Annual International Conference of the IEEE EMBSBuenos Aires, Argentina.

Zulpe, N., & Pawar, V. (2012), "GLCM Textural Features for Brain Tumor Classification", IICSI International Journal of Computer Science issues, Vol. 9, Issue 3, pp. 354-359

APPENDIX A

Table 1: Classifier target and corresponding output response for test Healthy Images sample

TEST SAMPLES	TARGET	OUTPUT
1	1 (Healthy)	1 (Healthy)
2	1 (Healthy)	1 (Healthy)
3	1 (Healthy)	1 (Healthy)
4	1 (Healthy)	1 (Healthy)
5	1 (Healthy)	1 (Healthy)
6	1 (Healthy)	1 (Healthy)
7	1 (Healthy)	1 (Healthy)
8	1 (Healthy)	1 (Healthy)
9	1 (Healthy)	1 (Healthy)
10	1 (Healthy)	1 (Healthy)
11	1 (Healthy)	1 (Healthy)
12	1 (Healthy)	1 (Healthy)
13	1 (Healthy)	1 (Healthy)
14	1 (Healthy)	1 (Healthy)
15	1 (Healthy)	1 (Healthy)
16	1 (Healthy)	1 (Healthy)
17	1 (Healthy)	1 (Healthy)
18	1 (Healthy)	1 (Healthy)
19	1 (Healthy)	1 (Healthy)
20	1 (Healthy)	1 (Healthy)

Table 2: Classifier target and corresponding output response for test DR Images sample

TEST SAMPLES	TARGET	OUTPUT
1	2 (Diabetic)	2 (Diabetic)
2	2 (Diabetic)	2 (Diabetic)
3	2 (Diabetic)	2 (Diabetic)
4	2 (Diabetic)	2 (Diabetic)
5	2 (Diabetic)	2 (Diabetic)
6	2 (Diabetic)	2 (Diabetic)
7	2 (Diabetic)	2 (Diabetic)
8	2 (Diabetic)	2 (Diabetic)
9	2 (Diabetic)	3 (Glaucoma)
10	2 (Diabetic)	2 (Diabetic)
11	2 (Diabetic)	2 (Diabetic)
12	2 (Diabetic)	2 (Diabetic)
13	2 (Diabetic)	2 (Diabetic)
14	2 (Diabetic)	2 (Diabetic)
15	2 (Diabetic)	2 (Diabetic)
16	2 (Diabetic)	2 (Diabetic)
17	2 (Diabetic)	2 (Diabetic)
18	2 (Diabetic)	2 (Diabetic)
19	2 (Diabetic)	2 (Diabetic)
20	2 (Diabetic)	3 (Glaucoma)

Table 3: Classifier target and corresponding output response for test Glaucoma Images sample

TEST SAMPLES	TARGET	OUTPUT
1	3 (Glaucoma)	3 (Glaucoma)
2	3 (Glaucoma)	3 (Glaucoma)
3	3 (Glaucoma)	3 (Glaucoma)
4	3 (Glaucoma)	3 (Glaucoma)
5	3 (Glaucoma)	3 (Glaucoma)
6	3 (Glaucoma)	3 (Glaucoma)
7	3 (Glaucoma)	3 (Glaucoma)
8	3 (Glaucoma)	3 (Glaucoma)
9	3 (Glaucoma)	3 (Glaucoma)
10	3 (Glaucoma)	2 (Diabetic)
11	3 (Glaucoma)	3 (Glaucoma)
12	3 (Glaucoma)	3 (Glaucoma)
13	3 (Glaucoma)	3 (Glaucoma)
14	3 (Glaucoma)	3 (Glaucoma)
15	3 (Glaucoma)	3 (Glaucoma)
16	3 (Glaucoma)	3 (Glaucoma)
17	3 (Glaucoma)	3 (Glaucoma)
18	3 (Glaucoma)	3 (Glaucoma)
19	3 (Glaucoma)	3 (Glaucoma)
20	3 (Glaucoma)	3 (Glaucoma)